Tree-ring width and density data around the Northern Hemisphere: Part 1, local and regional climate signals

Article *in* The Holocene · November 2002

DOI: 10.1191/0959683602hl587rp

CITATIONS
285

READS
286

6 authors, including:

Timothy John Osborn
University of East Anglia
176 PUBLICATIONS **16,319** CITATIONS
SEE PROFILE

Fritz H. Schweingruber
Swiss Federal Institute for Forest, Snow and Landscape Research WSL
253 PUBLICATIONS **15,686** CITATIONS
SEE PROFILE

P. D. Jones
University of East Anglia
605 PUBLICATIONS **75,396** CITATIONS
SEE PROFILE

S. G. Shiyatov
Russian Academy of Sciences
55 PUBLICATIONS **4,075** CITATIONS
SEE PROFILE

The Holocene 12,6 (2002) pp. 737–757

Tree-ring width and density data around the Northern Hemisphere: Part 1, local and regional climate signals

Keith R. Briffa,[1]* Timothy J. Osborn,[1] Fritz H. Schweingruber,[2] Philip D. Jones,[1] Stepan G. Shiyatov[3] and Eugene A. Vaganov[4]

([1]Climatic Research Unit, University of East Anglia, Norwich NR4 7TJ, UK; [2]Swiss Federal Institute of Forest, Snow and Landscape Research, Zurcherstrasse 111, CH-8903, Birmensdorf, Switzerland; [3]Institute of Plant and Animal Ecology, Ural Division of the Russian Academy of Sciences, 8 Marta Street 202, Ekaterinburg 620219, Russia; [4]Institute of Forest, Siberian Division of the Russian Academy of Sciences, Akagemgorodok, Krasnoyarsk 660036, Russia)

ADVANCE-10K

A

HOLOCENE

SPECIAL

ISSUE

Abstract: A detailed description is presented of the statistical patterns of climate forcing of tree growth (annual maximum latewood density and ring-width time series), across a network of 387 specially selected conifer sites that circle the extra-tropical Northern Hemisphere. The influence of summer temperature dominates growth. A mean April–September response is optimum for describing the major forcing signal over the whole densitometric network, though a shorter June–July season is more relevant in central and eastern Siberia. The ring-width chronologies also have a shorter optimum (June–August) seasonal signal, but this is much weaker than the density signal. The association between tree-ring density and precipitation variability (as measured by partial correlations to account for the correlation between temperature and precipitation) is considerably weaker than with temperature. The ring-width response to precipitation is dominated by 'noise' and local site influences, though a negative response to winter precipitation in northern Siberia is consistent with the suggestion of an influence of delayed snowmelt. Average correlations with winter temperatures are small for all regions and correlations with annual temperatures are positive only because of the strong link with summer temperatures. Reconstructions of summer temperature based on composite regional density chronologies for nine areas are presented. Five regions (northwestern North America, NWNA; eastern and central Canada, ECCA; northern Europe, NEUR; northern Siberia, NSIB; and eastern Siberia, ESIB) constitute an arbitrary 'northern' division of the network, while the four other regions (western North America, WNA; southern Europe, SEUR; central Asia, CAS; and the Tibetan Plateau, TIBP) make up the 'southern' part. We also present two larger composite regional reconstructions comprising the data from the five higher-latitude (HILAT) and four lower-latitude (LOLAT) areas respectively; and a single series made up of data from all regions (ALL), which is highly correlated with Northern Hemisphere mean summer temperature. We calculate time-dependent uncertainty ranges for each of these reconstructions, though they are not intended to represent long timescales of temperature variability (>100 years) because the technique used to assemble the site chronologies precludes this. Finally, we examine in more detail the reduced sensitivity in the tree-growth data to decadal-timescale summer-temperature trends during the last 50 years, identified in earlier published work.

Key words: Dendroclimatology, tree-ring width, tree-ring density, regional climate, summer temperature, Northern Hemisphere, late Holocene.

Introduction

During the 1980s and 1990s, tree-core samples were collected at hundreds of relatively cool and moist sites, effectively circling the mid- to high latitudes of the Northern Hemisphere (Schweingruber and Briffa, 1996). The tree cores were processed and measured to obtain a range of tree-growth parameters (Schweingruber, 1988), including total ring width (TRW) and maximum latewood density (MXD). The long-term aim of this work has been to provide the basis for reconstructing a multicentury history of interannual

*Author for correspondence (e-mail: k.briffa@uea.ac.uk)

10.1191/0959683602hl587rp

temperature variability that is continuous, annually resolved and exactly dated (Schweingruber and Briffa, 1996). Hence the network of tree-ring data contains a record of temperature changes that have occurred on interannual, decadal and longer timescales. The results can be expressed at different levels of spatial resolution ranging from the local site, through large regions and continents, up to the near-hemispheric scale. Briffa *et al.* (1988a; 1998b) used an earlier subset of these data to produce regional and 'hemispheric-wide' average series which they correlated against instrumental temperatures from co-located regions, identifying optimal seasonal averages of the temperature data: a six-month April–September season for MXD; and a three-month June–August season for TRW. A key result was the identification of a 'non-temperature' signal in both parameters, but particularly in the MXD data, causing a decline in the strength of the correlation with decadally smoothed temperatures in recent decades (Briffa *et al.*, 1998b).

The purpose of the present paper, which is the first part of a two-part series describing the climatic interpretation of the densitometric chronology network, is to present a detailed review of the statistical associations between interannual tree growth and observed temperature and precipitation variability registered at different temporal and spatial scales around the Northern Hemisphere. In this first part, we also present the time-series of tree growth averages for different subcontinental regions, calibrated against modern instrumental temperature so as to represent large regional-scale growing-season (April–September) temperature variations for the period from AD 1400 onwards. We provide time-dependent confidence limits for these proxy temperature series, making allowance for their changing makeup and diminishing internal replication as one goes further back in time.

We first describe the tree-ring and instrumental climate data and provide details of the methods by which they are compared. The pattern of response of the individual tree chronologies to different monthly and seasonal temperature and precipitation averages is presented. The climate signals present in the tree-ring data set at the regional scale are identified, and regional growing-season temperature reconstructions are built for the last 600 years. In the companion paper (Briffa *et al.*, Part 2, this issue), we present a series of detailed spatial reconstructions of summer temperature for each year from 1600 to 1887, and go on to describe the associations between the major patterns of tree-ring density variability and large-scale patterns of temperature, precipitation and surface-pressure data.

Data and method

Tree-ring data

We examine the climate sensitivities of tree growth at a total of 387 locations (Figure 1), looking separately at chronologies of the two most commonly used dendroclimatic growth parameters: maximum latewood density (MXD) and total ring width (TRW). Each chronology is a time series of annually averaged indices derived from measurements on a number of tree increment cores (around 20 or more per site). Here, the indices are residuals from a generalized exponential function, or 'Hugershoff', fitted through each original series of measurements (Bräker, 1981; Cook *et al.*, 1990). This indexing (or 'standardization') removes most of the multicentury-timescale variance, which mainly results from internal tree-growth processes that typically produce narrower and less dense rings as a tree ages. Such standardization also results in the loss of long-timescale variance that might be caused by changing climate (Cook *et al.*, 1995; Briffa *et al.*, 1996). Hence, our review of the climate sensitivities of tree growth within this network focuses on common variability that encompasses interannual, decadal and multidecadal to century timescales, but does not explore the association between tree growth and climate over longer (i.e., multicentury) periods. These aspects are described elsewhere (Briffa *et al.*, 2001).

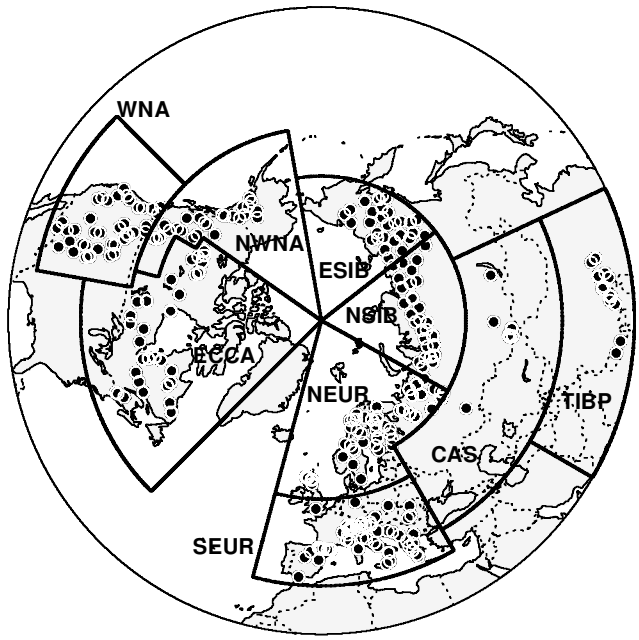

Figure 1 Location (circles) of the 387 sites with tree-ring width and density chronologies, together with the boundaries of the nine regions: NEUR = northern Europe; SEUR = southern Europe; NSIB = northern Siberia; ESIB = eastern Siberia; CAS = central Asia; TIBP = Tibetan Plateau; WNA = western North America; NWNA = northwestern North America; and ECCA = eastern and central Canada.

Climate data

The instrumental-based data used here to represent 'actual' temperatures at the locations of our chronologies are taken from the global set of monthly mean anomalies (with respect to 1961–90) available on a 5° latitude by 5° longitude grid-box basis from 1851 (Jones, 1994; Jones *et al.*, 1999). These data are derived from land stations only and contain no sea-surface or marine-air temperatures. For precipitation we use monthly totals, again for land only, originally interpolated onto a 0.5° latitude by 0.5° longitude grid (New *et al.*, 2000), but regridded to correspond directly with the (lower) spatial resolution of the temperature data.

Statistical characterization of climate 'signals'

We have based this analysis on simple correlation, i.e., Pearson correlation coefficients calculated between each chronology and both the temperature and precipitation records from the grid box in which it lies, for each of the successive monthly climate series representing June of the year prior to tree growth up to September of the year of growth: a total of 16 individual monthly correlations for temperature and 16 for precipitation. The signs and magnitudes of the significant coefficients characterize the pattern of climate forcing of tree growth: i.e., the dendroclimatic 'response function' (Fritts *et al.*, 1971; Blasing *et al.*, 1984; Briffa and Cook, 1990). The correlations are computed over the full period 1881–1984 for temperature, and 1901–84 for precipitation. The end year was chosen because many of the chronologies end after 1984 (a small number stop before this, but not enough to bias the results). For some grid boxes, the instrumental record length can be rather short; in those cases, a variance-adjusted average (Osborn *et al.*, 1997) is taken of any observations within the nine boxes (3 × 3) centred on the chronology location. All correlations, therefore, are based on at least 25 years (and mostly many more) of data within the 1881 to 1984 period.

In many areas, temperature and precipitation are positively cor-

related during winter and negatively correlated in summer, the latter particularly so in the more southern regions (Figure 2). Due to this dependence, we also computed partial correlations between the tree-ring variables and temperature (holding the precipitation constant) and precipitation (holding the temperature constant). Removing the influence of precipitation only slightly reduced the correlations between temperature and TRW or MXD, while the partial correlations between precipitation and the tree-ring variables were generally much lower. We conclude from this that temperature is the dominant growth-limiting factor in this network of chronologies and we present the results in terms of temperature correlations and precipitation *partial* correlations (i.e., treating the latter as a secondary influence). This is also the case for regional average correlations discussed later. However, we note that, at very large spatial scales, the correlation between temperature and precipitation can change in sign (see, e.g., Hulme *et al.*, 1998).

Chronology climate signals

Maximum latewood density

The 16 monthly temperature correlations for all 387 chronologies are too numerous to present individually, so principal component analysis (PCA) was applied to extract the major patterns of tree-growth response from within the (16 by 387) correlation coefficient matrix. The two major patterns of seasonal climate forcing of MXD are shown in Figure 3. The leading principal component (PC) is very dominant, capturing 59% of the variance, clearly demonstrating that strong positive correlations exist between MXD and local temperatures during each of the months from April through to September in the year of ring growth over virtually the whole of the chronology network (Figure 3b). There is also a negative but much weaker association with temperatures in the latter half of the previous growing season. Only in eastern Siberia and the Tibetan Plateau is this pattern of seasonal temperature forcing less strongly expressed (Figure 3a). Averaged monthly temperatures from April to September therefore represent the best overall expression of seasonal temperature forcing of MXD for the network as a whole. The second PC (Figure 3, c and d), accounting for just 8% of the variance, indicates enhanced sensitivity to June and July temperatures and reduced sensitivity to those in March, April and September. This emphasizes the predominant shorter midsummer growing-season response in the northern and eastern Siberian MXD chronologies, and the region with strong positive loadings on this PC corresponds closely to that where the growing season normally begins near to 1 June (see the 'day 150' contour in Figure 2 of Jones and Briffa, 1995).

Subsequent modes (not shown) become less spatially and seasonally coherent. The fourth (capturing 5%) suggests a response to an even shorter and somewhat later growing season in the far northeast of Siberia with the emphasis on July and August temperatures (see also Hughes *et al.*, 1999).

The individual site correlations can be averaged across groups defined, for example, by region or tree genus, to demonstrate underlying average climate responses. As not all genera of trees are present in all geographical regions, we have not attempted to separate the influence of region and genus. Nevertheless, for MXD, we find that *Larix* generally respond over a shorter growing season, while *Abies*, *Picea*, *Pinus*, *Pseudotsuga* and *Tsuga* correlate more strongly against six-month (April–September) mean temperatures. Though all genera exhibit a high degree of intersite variability in their correlations with seasonal-mean temperature, *Larix* and *Pinus* have the most chronologies with $r \geqslant 0.9$.

Averaging response patterns across all genera and species within regions (as defined in Figure 1) highlights the dominant geographic influence on MXD variability of spring and summer temperatures, much more so than temperatures in other months or precipitation in general (Figure 4). For each month, within each region, a range of individual-site temperature correlations is apparent (as shown by the filled triangles) but for the most part these are positive and of increasing magnitude throughout the spring and summer months, with their mean values (shown by the shaded bars) generally peaking in August in most regions. In TIBP and WNA the ranges of summer monthly correlations include more negative values, but the summer monthly means are again all positive. Finally, we note that in SEUR, TIBP, WNA, NWNA and ECCA there is some evidence of a bimodal MXD temperature response, with strong correlations with spring and late-summer temperatures, but less sensitivity to (typically) June temperatures (see also Schweingruber *et al.*, 1991).

The above analysis demonstrates that there is marked geographical variation in the response of the maximum latewood density to temperature, but that if one characteristic season is required (which is the case for certain applications) then the mean April–September temperature would be the optimal overall choice. Figure 5a summarizes association of the MXD data set with this six-month warm-season temperature. Almost 90 per cent of the chronologies have a correlation exceeding $r = 0.22$, which is the threshold indicating better than random association with 95% confidence, given that the average overlap between chron-

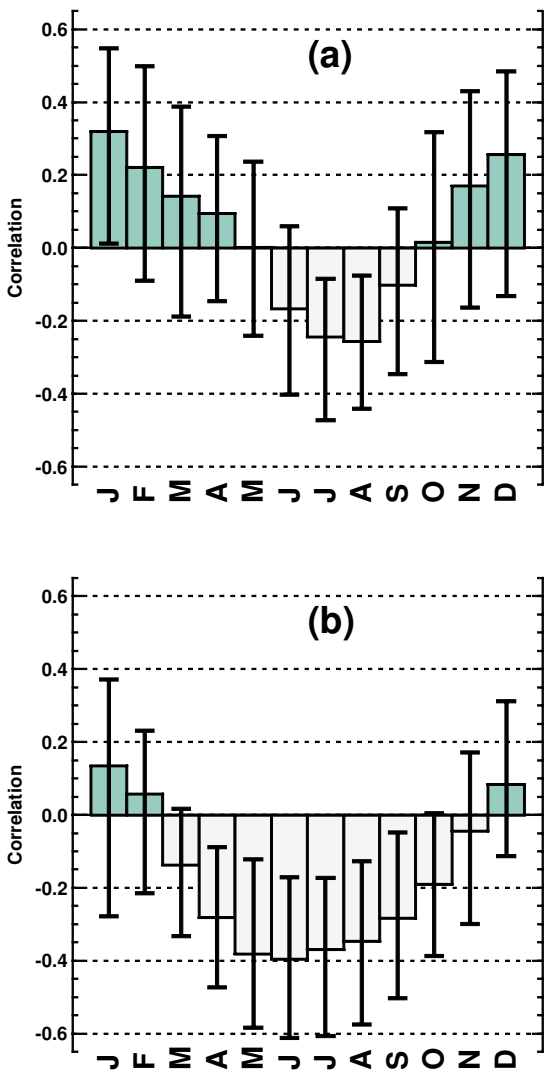

Figure 2 Correlations between grid-box monthly temperatures and precipitation, averaged over grid boxes falling into (a) the high-latitude regions (NWNA, ECCA, NEUR, NSIB and ESIB) and (b) the lower-latitude regions (WNA, SEUR, CAS and TIBP). The histograms show the mean of the individual correlations averaged over the regions, while the lines and bars indicate the 5 to 95 percentile range.

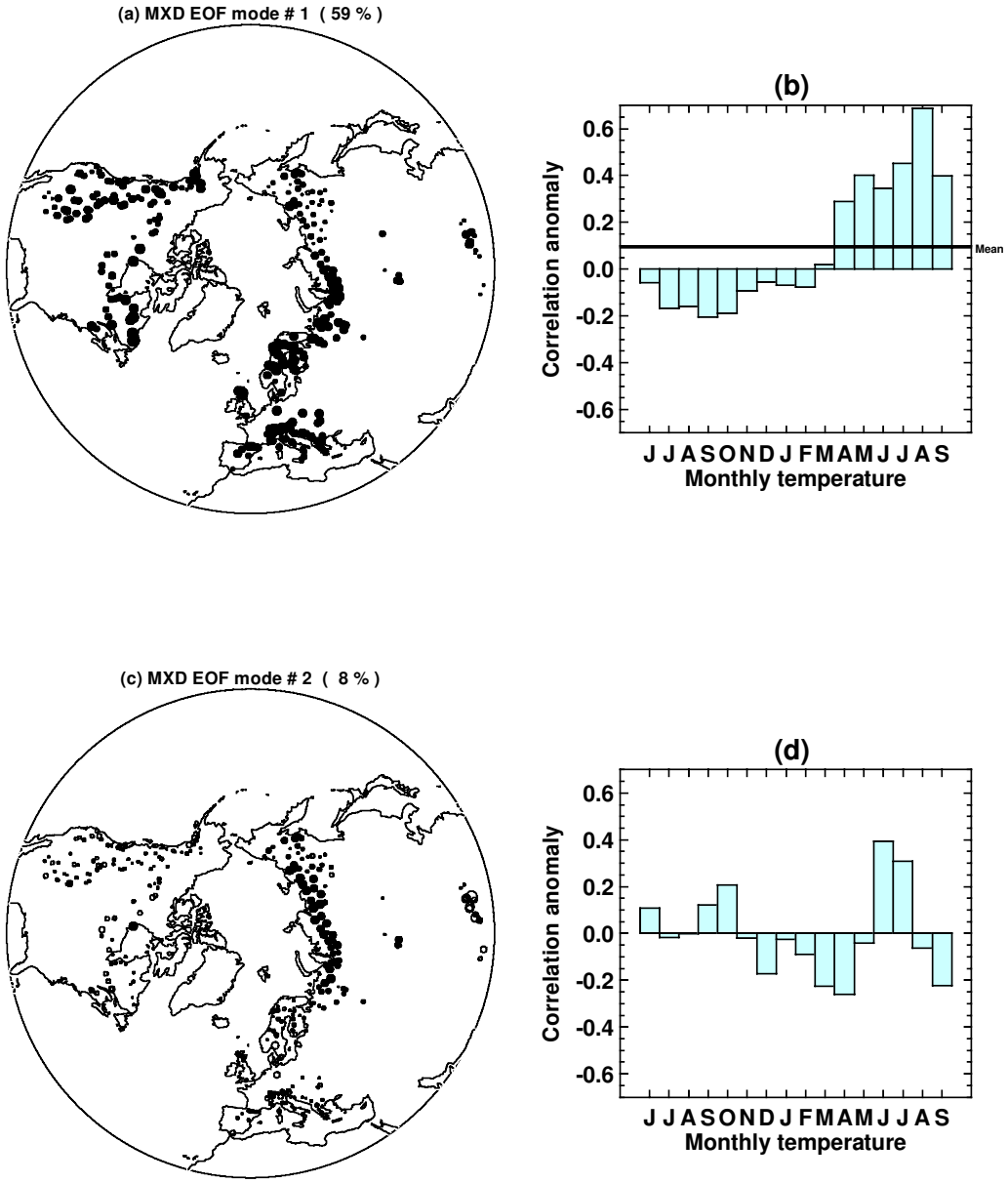

Figure 3 (a, b) First and (c, d) second principal components of the array of correlations (between each MXD chronology and each monthly temperature from the previous June to the concurrent September). Parts (a) and (c) show the loadings on each component, solid circles positive and open circles negative, diameter proportional to loading. Parts (b) and (d) show the component in terms of the correlations between MXD and monthly temperatures. The mean correlation across all months and all sites was subtracted prior to analysis, and was subsequently added back to the first component (it is marked in (b)).

ology and instrumental data provides a sample of 81 years. The highest correlations are clustered in Europe and central northern Siberia, with a scattering across North America. The lower correlations in eastern Siberia partly reflect that this is a non-optimal season for that region.

Applying PCA to the matrix of partial correlation coefficients between MXD and monthly precipitation demonstrates that the precipitation signal is much less coherent. The first two modes (Figure 6) capture just 19% and 12% of the variations in correlation (compared to 59% and 8% for temperature), and, after those two, the modes degenerate into spatial and seasonal incoherence. The leading mode shows that a number of chronologies have positive correlations with precipitation during the previous growing season, and negative correlations with July and August precipitation during the growing season in the year of ring growth (Figure 6b). This seasonal signal has positive loadings across widely distributed sites, but with *some* sites in western USA and southern Europe exhibiting the strongest loadings (Figure 6a). The second mode (Figure 6, c and d) indicates positive correlations between winter (October to January) precipitation and MXD in southern Europe, and negative correlations with MXD in northwestern Siberia. The former signal demonstrates a dependence of growth on the moisture availability during the winter season in southern Europe. The latter signal is consistent with the mechanism suggested by Vaganov *et al.* (1999) that enhanced winter snowfall leads to delayed snowmelt and hence affects the initiation of tree growth. The results imply, however, that this mechanism only has a strong impact on maximum latewood density in a very limited region of northern Siberia (Figure 6c).

There is little dependence at the tree genus level in the response of MXD to monthly precipitation. The range of monthly partial correlations within each genus group generally spans zero, with

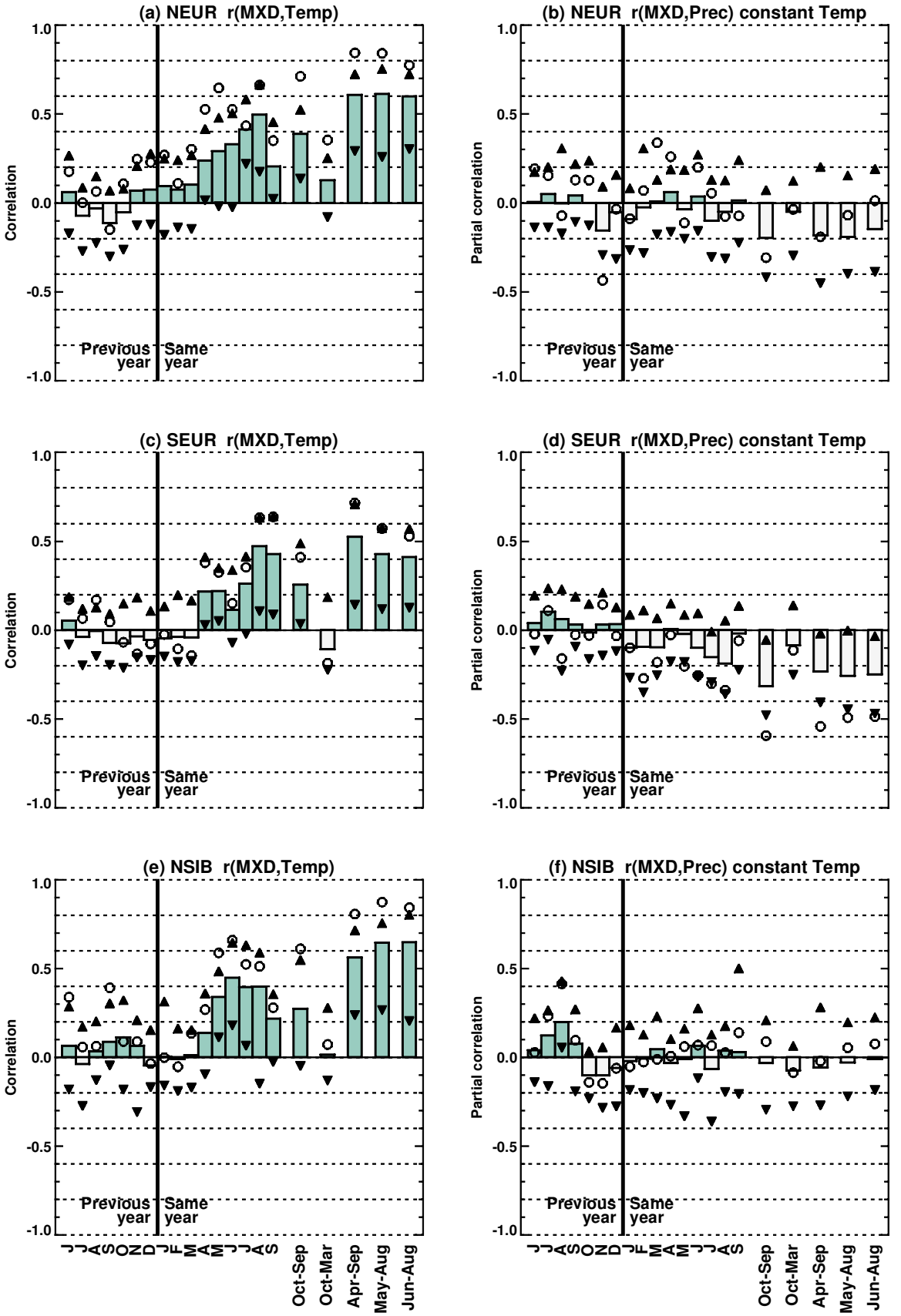

Figure 4 Correlations (1881–1984) between individual MXD chronologies and monthly temperatures (a, c, e, g, i, k, m, o, and q), or partial correlations between MXD and monthly precipitation, holding temperature constant (b, d, f, h, j, l, n, p and r), averaged across the regions defined in Figure 1. Also shown are correlations (or partial correlations) with five selected seasonal-mean temperatures or precipitation totals (October to September, October to March, April to September, May to August and June to August). Each histogram indicates the mean, with triangles indicating two standard deviations about the mean (based on the intra-region variation in correlation). Circles indicate the corresponding correlations (1881–1960) obtained when (a subset of) the MXD and temperature or precipitation are averaged into regional means first.

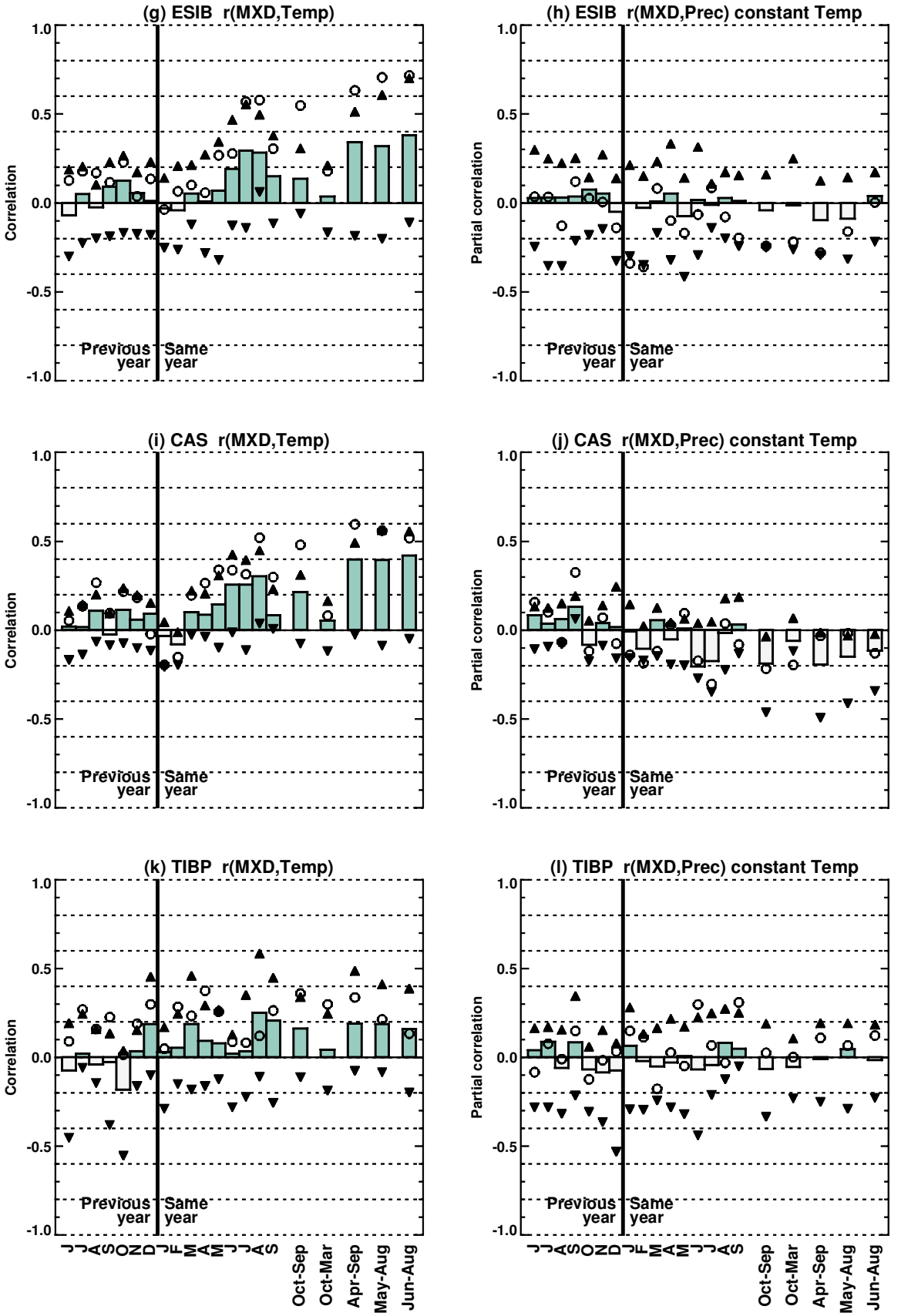

Figure 4 Continued.

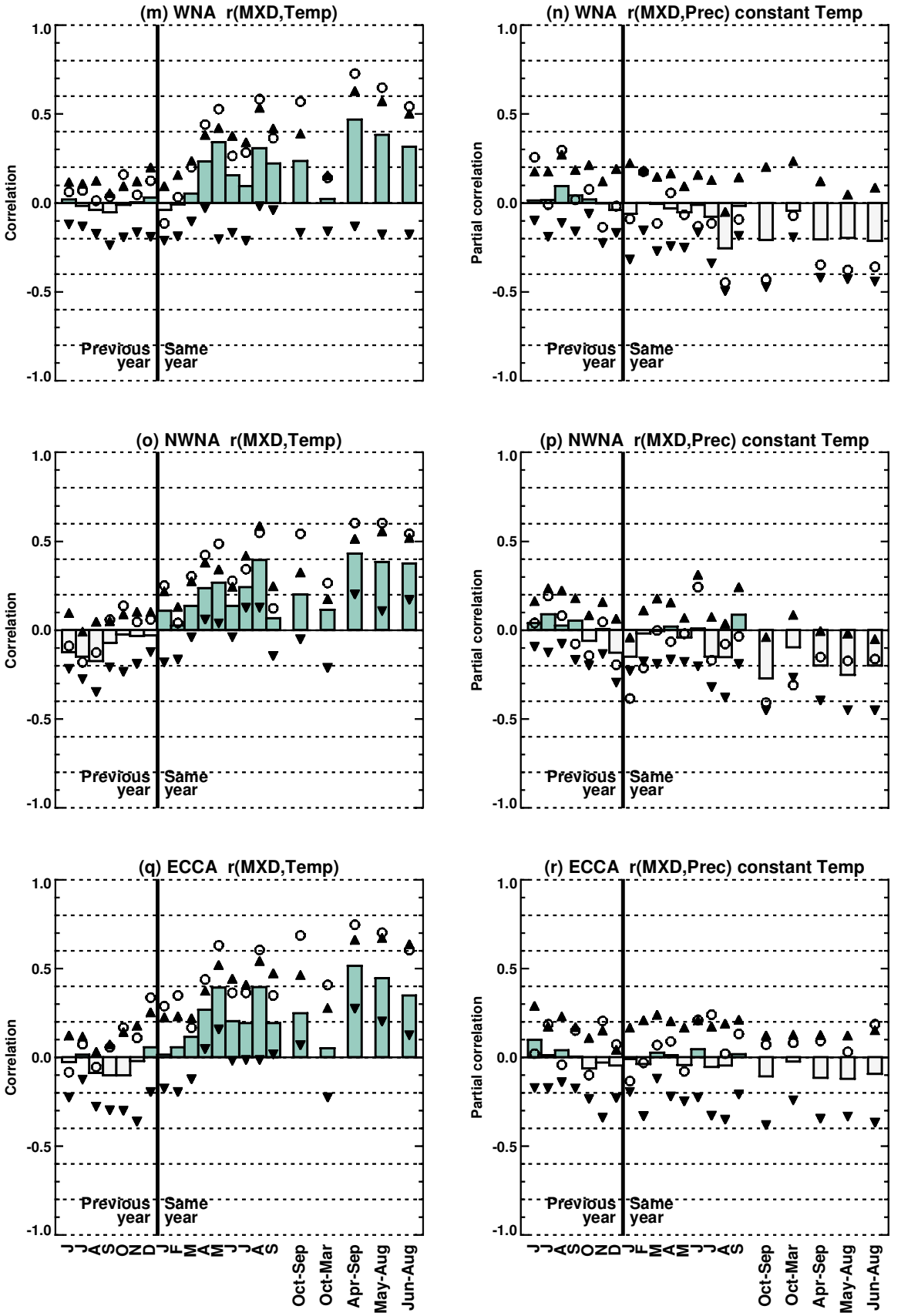

Figure 4 Continued.

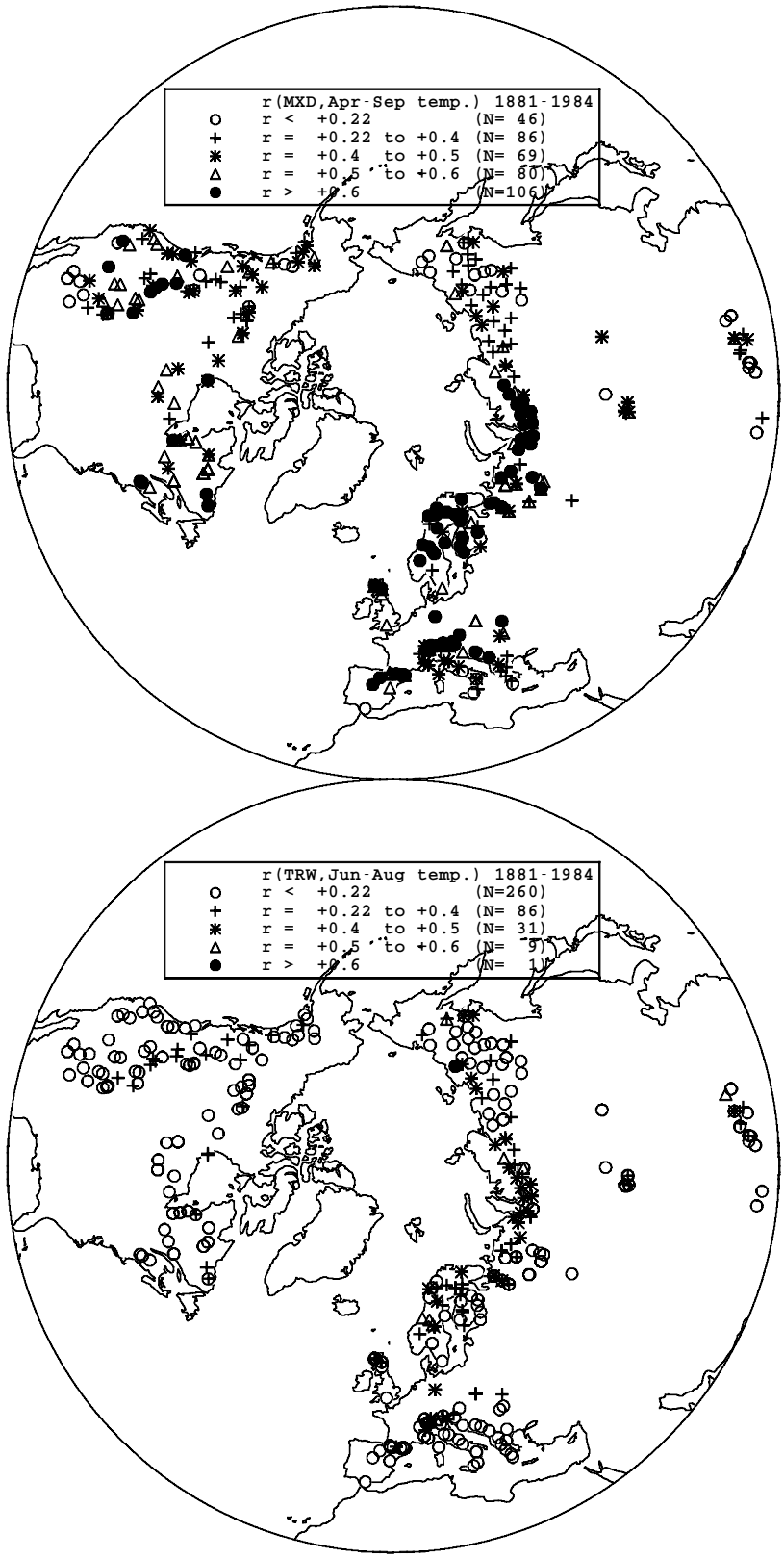

Figure 5 Correlations between (a) April to September mean temperatures and MXD chronologies, and (b) June to August mean temperatures and TRW chronologies, computed over 1881 to 1984, with symbols indicating correlation (open circle = $r < 0.22$; + = $r < 0.4$; * = $r < 0.5$; triangle = $r < 0.6$; solid circle = $r > 0.6$). The key also indicates the number of chronologies in each category.

a slight bias towards negative correlations with monthly precipitation during the growing season, a bias that becomes slightly stronger for all genera when precipitation is totalled over the growing season. The negative correlations demonstrate that none of the genera are limited by summer moisture availability in this data set.

Averaging responses to precipitation across all chronologies within each region (Figure 4) demonstrates that the negative partial correlations with growing-season precipitation are stronger in Europe and North America than in Asia, but that nonetheless they remain weak relative to the influence of temperature. The regional-mean response functions fail to capture the characteristics identified by the second principal component (Figure 6, c and d), because the regional definitions (Figure 1) split the north-

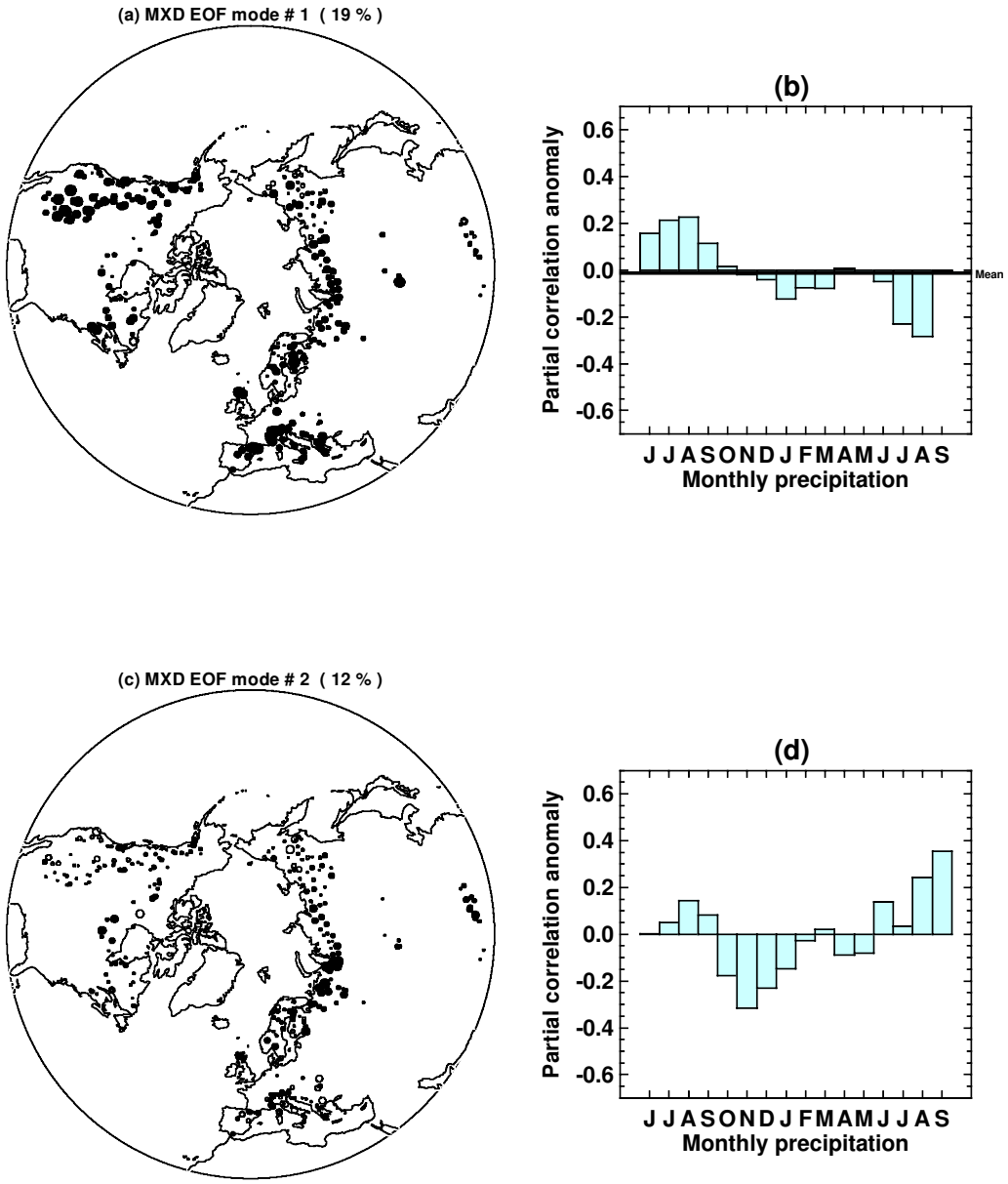

Figure 6 As Figure 3, but for the partial correlations between MXD and monthly precipitation (holding temperature constant).

western Siberia winter snowfall signal between NEUR and NSIB and combine them with chronologies that do not show the same characteristic response to precipitation. This emphazises the value of the PCA approach.

Total ring width

The ring-width chronologies also depend most strongly on summer temperature, but the PCA (Figure 7) identifies a much shorter overall response season (June to August). Although the leading component has positive loadings across much of the network, the loadings and the correlation anomalies are generally weaker than for MXD (Figure 7, a and b; cf. Figure 3, a and b) and the leading TRW component captures only 25% of the variance of the response functions. This gives an indication that the climate signal in the TRW is weaker or more heterogeneous than that for MXD. The leading TRW PC also combines the response of TRW to the short growing-season temperature with negative correlations for early spring and, particularly, previous growing-season temperatures.

The second PC (Figure 7, c and d) captures the distinct characteristics exhibited by most of the southern European chronologies (with the exception of those in the Alps), in that they are negatively correlated with previous growing-season temperatures and positively correlated with temperatures from November to April. The latter signal is of particular interest, given the relative scarcity of climate proxies that are sensitive to winter temperatures (Briffa and Jones, 1993; Jones *et al.*, 1998). Lower-order components are spatially or seasonally less coherent and are difficult to interpret meaningfully.

As with MXD, the temperature-response functions for TRW show large variability within region-based or genus-based groupings. Nevertheless, some interesting variations between the groups are discernible. *Larix* generally have the strongest correlations with summer temperatures; these are located predominantly in the NSIB and ESIB regions, explaining the moderately strong summer response in these regions (Figure 8, e and g). Against summer temperatures, *Tsuga*, *Picea* and *Pinus* have somewhat weaker correlations than *Larix*; *Abies* has an average correlation near zero; while the 11 *Pseudotsuga* chronologies in western North America exhibit significant negative correlations. All genera except *Larix* show negative correlations with the previous growing-season temperatures, also apparent in the regional groupings for Europe and North America (Figure 8, a, c, m, o and q). The northern Eurasian regions (NEUR, NSIB, ESIB and CAS) show most clearly the strongest response to the shorter (June to August) seasonal-mean temperature. At a more local site level, ring-width

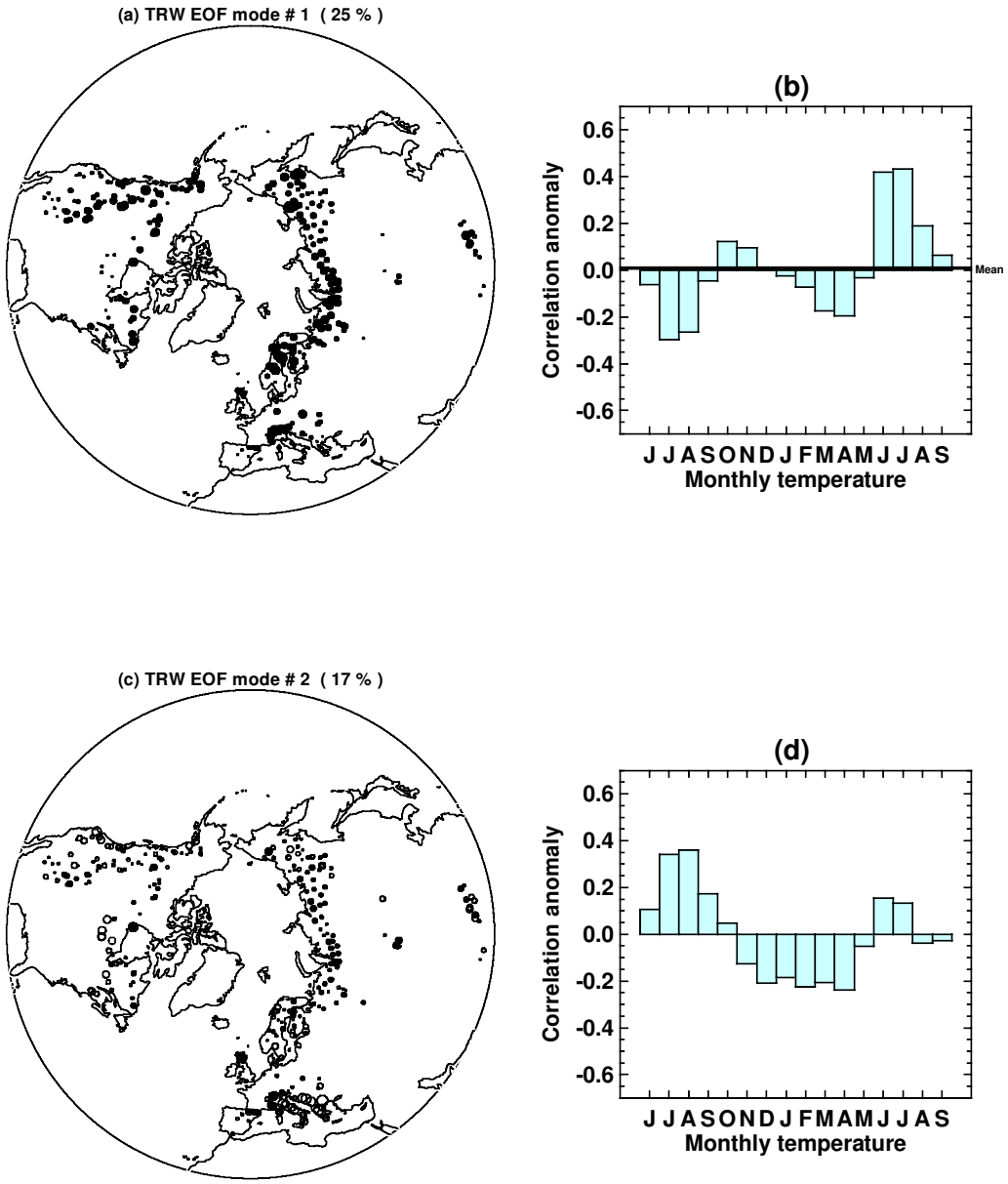

Figure 7 As Figure 3, but for the correlations between TRW and monthly temperatures.

correlations with temperature can be significantly higher than is indicated in the large regional averages incorporated in Figure 8, as has been shown for a much narrower seasonal window in some northern Eurasian sites by Hughes *et al.* (1999) and Vaganov and Shashkin (2000).

The response of TRW to precipitation variations is very weak (Figure 8) and is generally dominated by noise and local site influences. The only exception is that the first component (Figure 9) obtained from the PCA of the TRW-precipitation partial correlation structure shows a cluster of northern Siberian chronologies that are negatively correlated with winter precipitation (see also Mazepa, 1999). This provides regional support for the 'enhanced snowfall = delayed growth' mechanism suggested by Vaganov *et al.* (1999), for a larger region than the similar signal in the maximum latewood density chronologies (Figure 6, c and d). The NSIB regional average (Figure 8f) shows this signal as a small negative shift in the range and mean of the chronology correlations with winter precipitation.

The large-scale response of the TRW chronologies to climate is generally weaker and more heterogeneous than for MXD. This makes the selection of a single optimal season harder. On the basis of Figure 7(a and b), however, a June and July or a June–August mean temperature appears to be suitable. Figure 5b shows the site-by-site correlations between the TRW chronologies and the June–August mean temperature. In comparison with MXD (Figure 5a), the climate signal is clearly very much weaker, with two-thirds of the chronology correlations not significant at the 95% confidence level. The highest correlations are all located in Eurasia, particularly in the northern regions. Only 10 TRW chronologies have correlations with the June–August temperature that exceed $r = 0.5$, compared to 186 MXD chronologies (correlated with April–September temperature).

Regional and hemispheric climate signals and reconstructions

Regional climate signals

The dominant climate signal in the MXD and TRW data sets was identified above to be the growing-season temperature, with optimal seasons of April to September for MXD and June to August for TRW. The chronology-temperature correlations (Figure 5) demonstrate useful skill for reconstructing past temperature variations, but the correlations can be increased by combining the chronologies and temperature observations into regional series, because the regional averaging increases the signal-to-noise ratio,

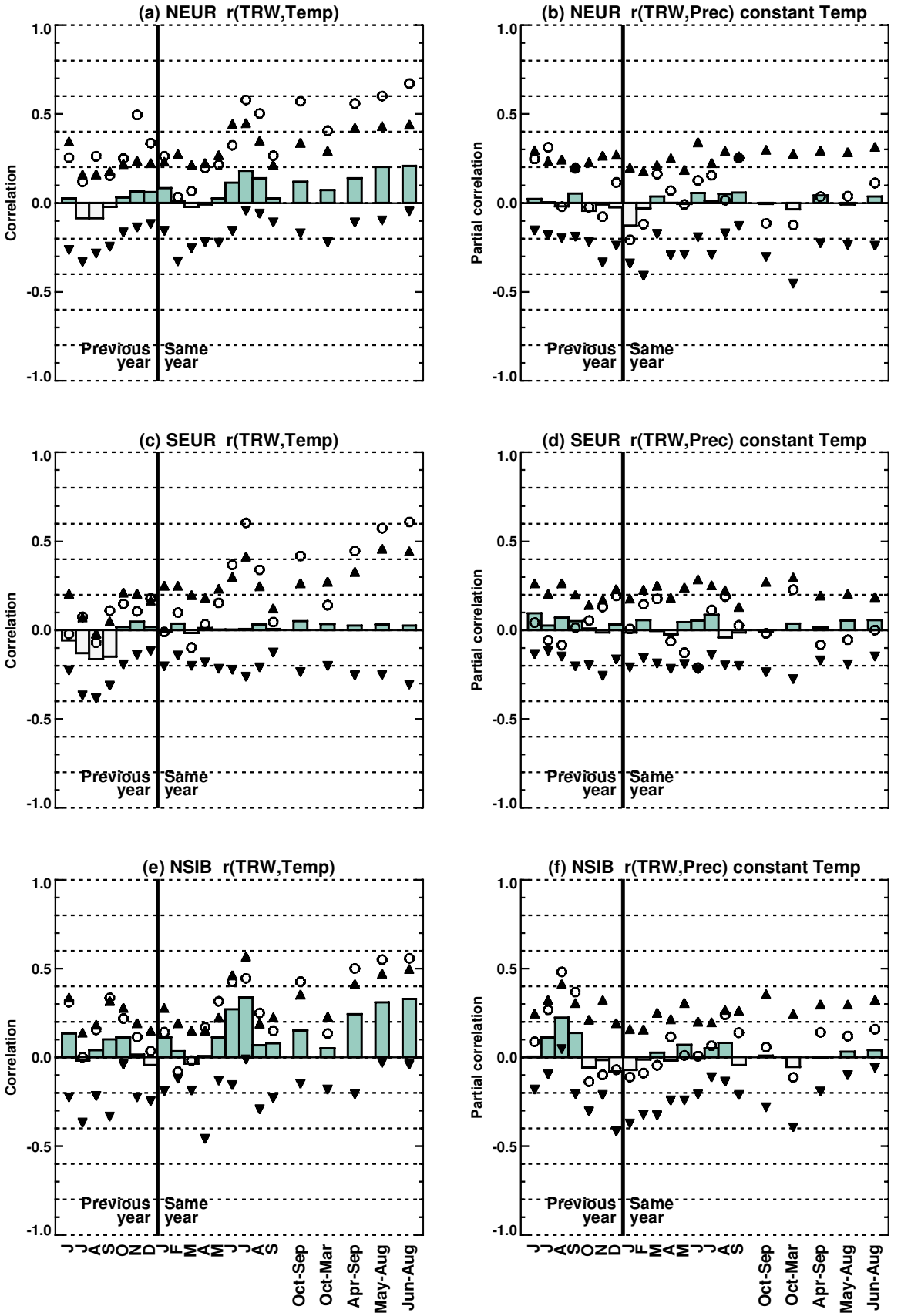

Figure 8 As Figure 4, but showing the correlation between TRW and monthly and seasonal temperature and precipitation.

in the same way that averaging of individual tree cores at a site yields the common signal at the expense of locally generated noise.

The regional temperature and precipitation series are computed as area-weighted averages of all land grid-boxes within each region (Figure 1) that have instrumental data and that contain at least one tree-ring chronology site. The regional means have their variance adjusted to compensate for the effects of time-dependent observational coverage (Osborn *et al.*, 1997). The regional tree-ring density and width series are computed as weighted averages of the chronology time series (with time-dependent weighting based on the number of tree cores contributing to each yearly

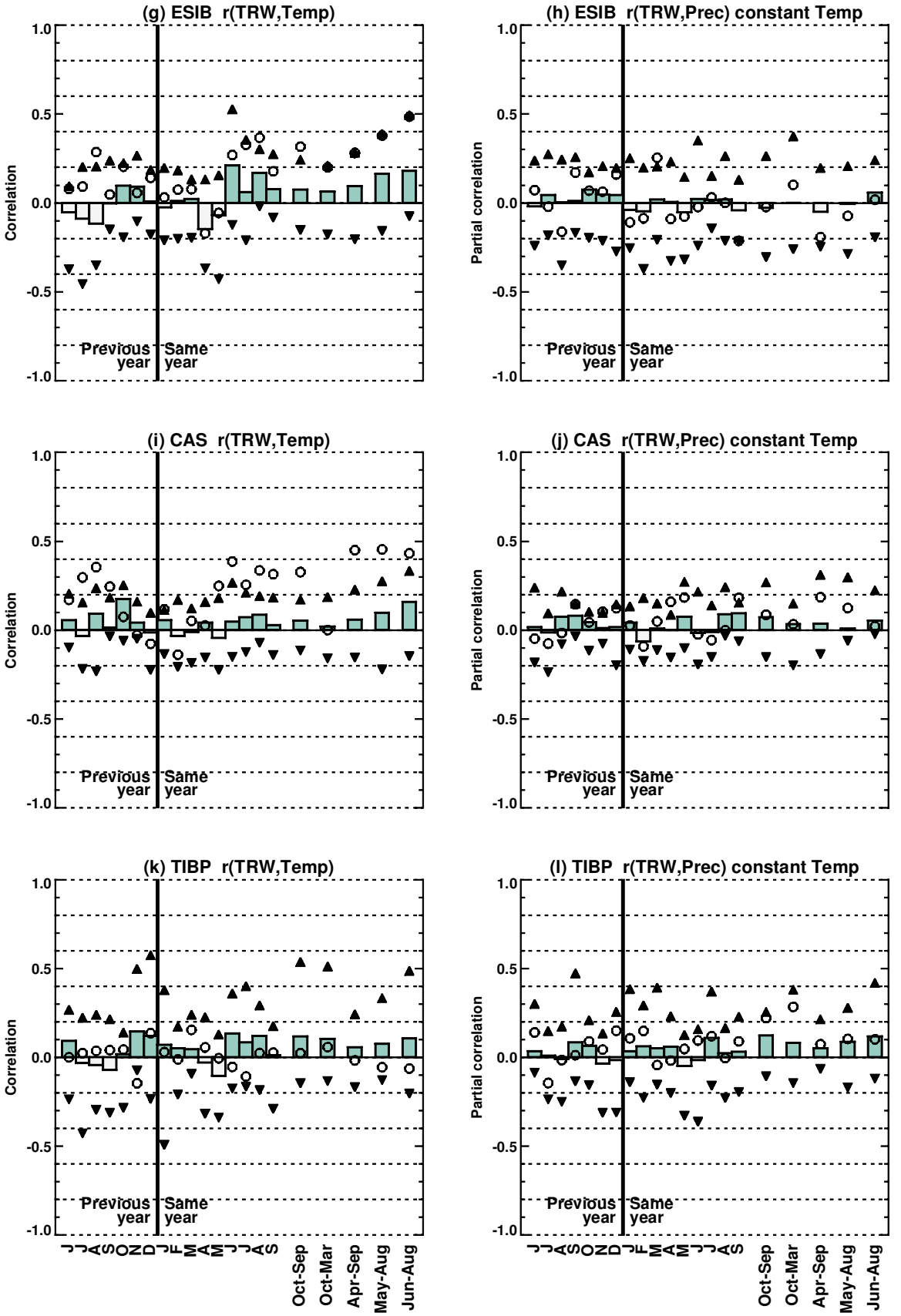

Figure 8 Continued.

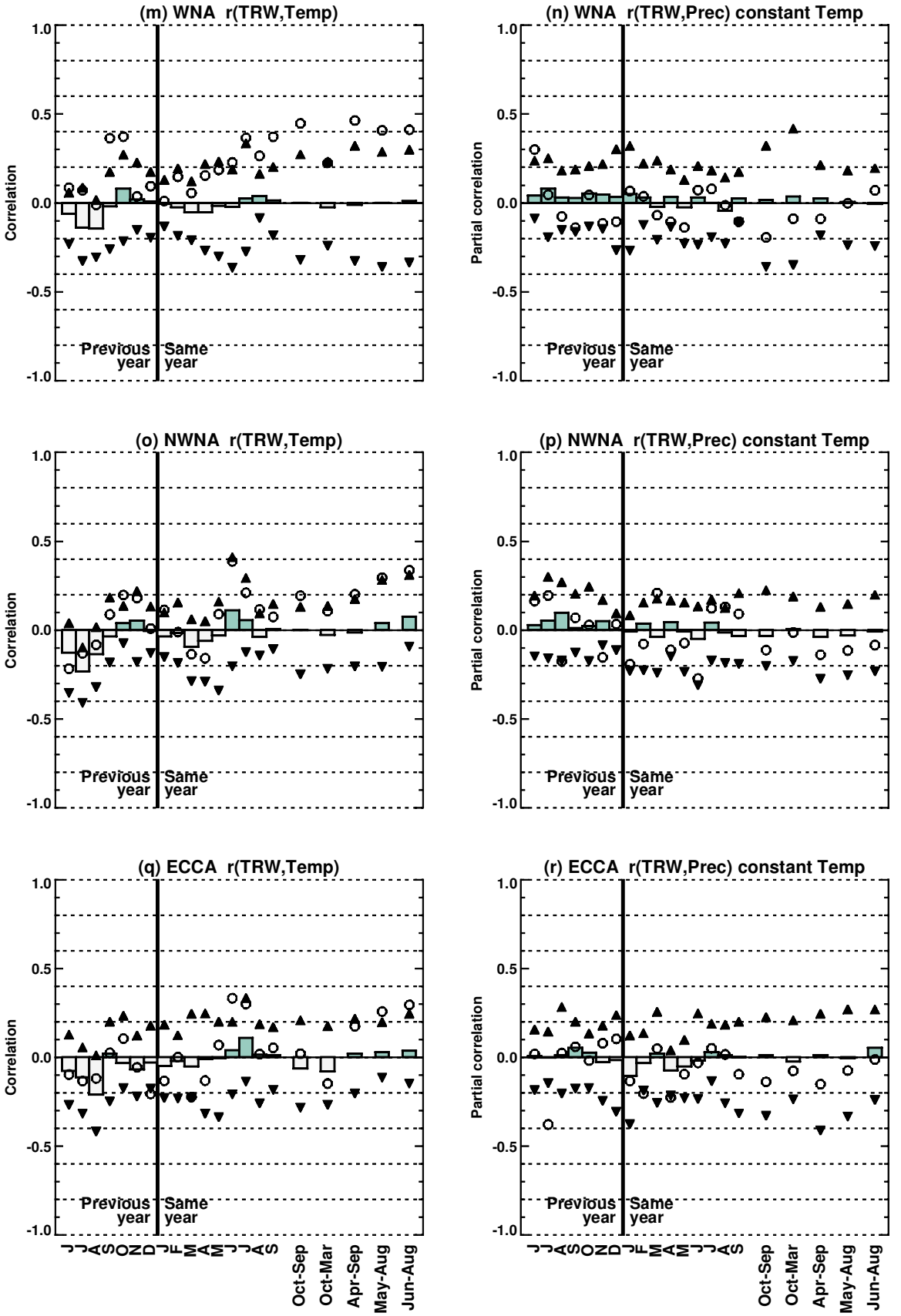

Figure 8 Continued.

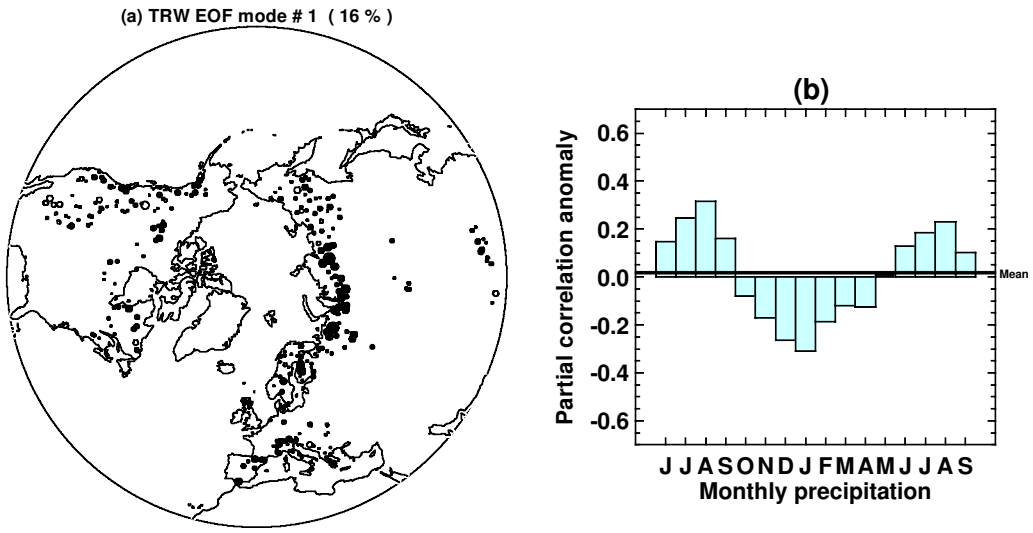

Figure 9 As Figure 3, but for the leading principal component only of the partial correlations between TRW and monthly precipitation (holding temperature constant).

chronology value), and then similarly adjusted to compensate for the effects on variance of changing numbers of chronologies through time (Osborn *et al.*, 1997). Various subsets of chronologies within each region, as described below, have been used to obtain alternative regional-mean time series, but the regional tree-ring series are *always* compared with the regional temperature or precipitation from grid boxes co-located with the *full* set of chronologies.

The correlations between regional-mean MXD or TRW and temperature are generally higher than the average of the individual chronology correlations, particularly for growing-season temperature. They are still somewhat degraded, however, by chronologies that have little apparent temperature sensitivity. If a subset of chronologies is selected, by removing the 46 MXD chronologies that have $r < 0.22$ with April–September local temperature (Figure 5a), or the 260 TRW chronologies that have $r < 0.22$ with June–August temperature (Figure 5b), then many of the regional means correlate much more strongly with regional-mean summer temperatures. For MXD the only notable improvement is in the ESIB region, due to the relatively high proportion of chronologies failing the $r \geq 0.22$ criterion (Figure 5a). For TRW, however, the subset of chronologies results in improved correlations with summer temperature in all regions except NSIB (where the strongest local signals occur for TRW), TIBP and ECCA (where very few chronologies pass the criterion).

Figure 4 shows (as open circles) the correlations between the various subsets of regional MXD time-series and the corresponding area-averaged monthly temperature and precipitation. The recent non-temperature signal (Briffa *et al.*, 1998b) in the tree-ring parameters becomes more apparent at the regional scale, so these correlations are computed using data from the period 1881–1960 only. In the spring and summer growing-season months, these are near or above the upper end of the range of individual site correlations, with the exception of the TIBP region. Average correlations against winter temperatures are small for all regions and correlations with mean annual temperatures are positive only because of the strong link with summer temperature. As expected from the individual chronology results (e.g., Figure 3), chronologies in SEUR and the North American regions correlate most strongly with the April–September temperature 'season' (see right-hand sections of Figure 4, c, m, o and q), while northern and eastern Siberia respond to the shorter June–August average (Figure 4, e and g). Other regions show less dependence on the precise seasonal definition.

The various subsets of regional TRW time series correlate more strongly with monthly temperatures than most of the individual chronologies did (Figure 8, open circles). The improvement is yet more noticeable when the temperatures are averaged over the growing season; against June–August temperature, the regional correlations are at or above the 95th percentile of the local correlations for eight of the nine regions, and are sufficiently high to offer useful reconstruction skill. The regional correlations of TRW with precipitation or with temperatures from outside the growing season shown in Figure 8 are not a good measure of the regional reconstruction potential of the TRW data set due to the many chronologies that have been discarded solely on the basis of their poor correlation with growing-season temperature.

Regional temperature reconstructions

Figures 4 and 8 indicate the potential for climate reconstruction at the regional scale based on the MXD and TRW data sets. A few of the individual chronologies have data back to at least AD 1400, but most of them do not. The skill of a reconstruction will depend upon the number of chronologies comprising each regional mean, and will therefore be time dependent. To evaluate this, regional time series of tree-ring density and width are computed using subsets of the chronologies that have data back to certain selected years (e.g., AD1600). As there is also a decline in the number of chronologies with data since 1980, the skill of the most recent years is assessed by using a subset of chronologies with data up to at least 1988. The chronologies in these subsets also have to pass the criterion used above, i.e., that their correlations with the local grid-box growing-season temperatures must be 0.22 or higher.

The regional MXD and TRW time series computed from these various subsets ('fixed grid' subsets, since the number of chronologies is no longer time-dependent) are correlated against the observed regional temperatures (April–September or June–August) over the 1881–1960 period (Figure 10). The correlations do decline for the earlier fixed grids, although often by only a moderate amount given the very small number of chronologies that have data prior to 1600. Tree-ring density is always superior to the total ring width, with the single exception of the southern Europe region based on those chronologies with data back to at least 1700. The MXD time series also extend further back in time for three of the regions, because many of the TRW chronologies were discarded for failing to correlate significantly with their local grid-box temperature.

In addition to the nine regions defined in Figure 1, three composite regional means are also generated. The 'HILAT' region combines all chronologies and temperatures from the five higher-

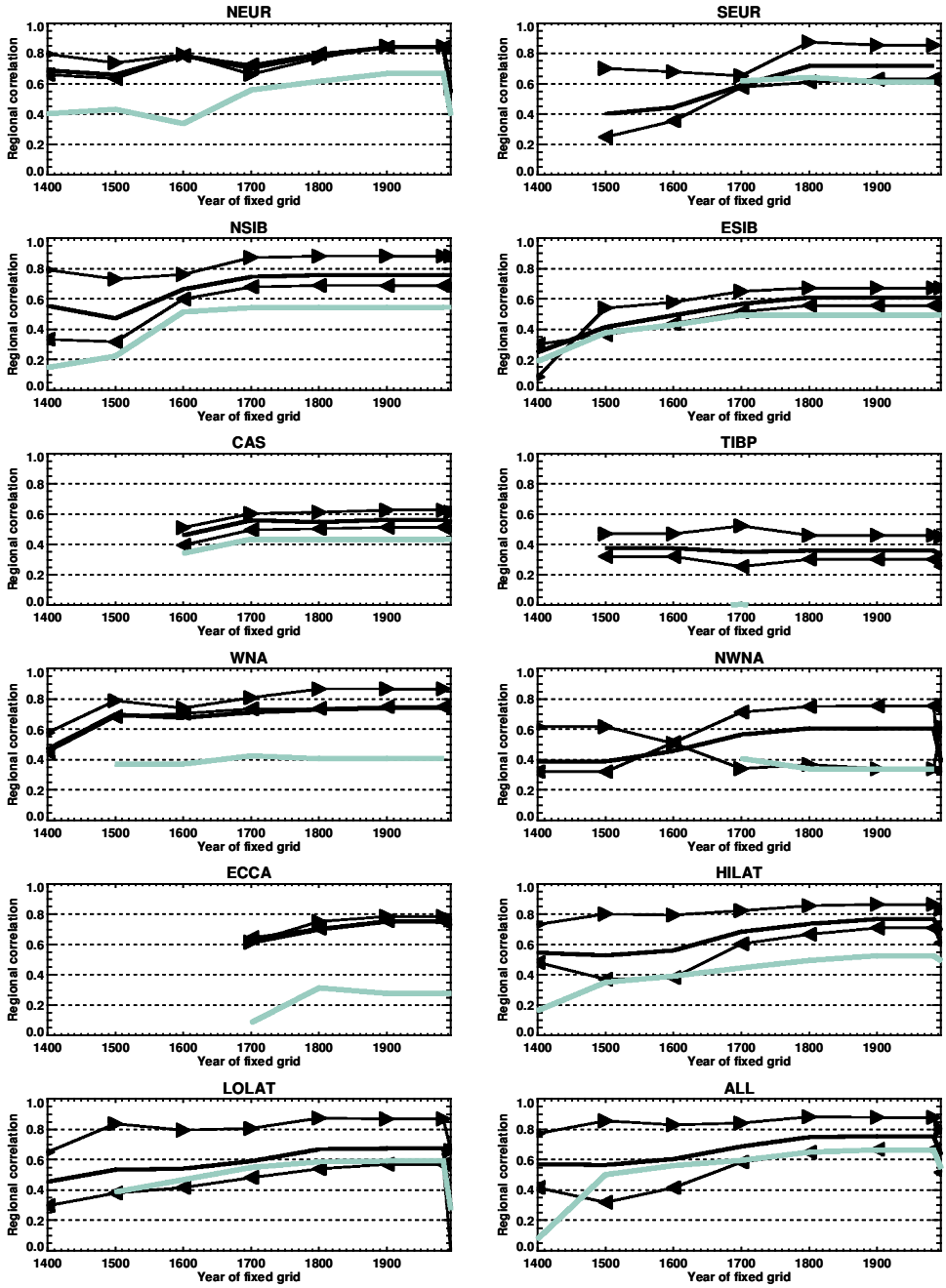

Figure 10 Correlations (1881–1960) between regionally averaged temperatures and regionally averaged TRW (grey lines) or MXD (black lines), where the regional-mean tree-ring time series are computed using a fixed subset of chronologies that have data back to a specified year, plotted against the specified year. The fixed subsets contain only those chronologies with data back to AD 1400, 1500, 1600, 1700, 1800, 1900, or with data continuing to 1978 or 1988. For MXD only, correlations are also shown after high (◀) or low (▶) pass filtering of the data, using a 10-year Gaussian-weighted filter. MXD is correlated with mean April to September temperatures, TRW with June to August temperatures.

latitude regions (NWNA, ECCA, NEUR, NSIB and ESIB), while 'LOLAT' combines the remaining four regions (WNA, SEUR, CAS and TIBP). The 'ALL' region is defined as the area-weighted average of all land temperature grid boxes with chronologies in them, and the average of all chronologies that pass the criterion of local temperature sensitivity ($r \geqslant 0.22$). The observed temperature time series for the 'ALL' region is highly correlated with Northern Hemisphere mean temperature and thus represents the near-hemispheric climate signal in the tree-ring data set.

For MXD, the correlations are higher for the HILAT region than for the LOLAT region, while the opposite is true for TRW. The additional averaging to produce the ALL regional means improves the signal-to-noise ratio further, resulting in correlations that are as high as, or higher than, the HILAT and LOLAT correlations. For the near-hemispheric ALL region, the TRW correlates almost as strongly as does the MXD series (back to 1500, prior to which no lower-latitude TRW data pass the criterion for inclusion and the TRW skill falls rapidly).

For the MXD time series, correlations with April–September temperature have also been computed after the time series have been high- or low-pass filtered (with a 10-year Gaussian-weighted filter). For almost all regions and fixed grids, the correlations between the low-pass filtered series are higher than those with the high-pass filtered series (Figure 10). The most notable exception to this is the NWNA region, for which the low-frequency correlations are much lower (although the small number of NWNA chronologies that have data back to 1400 or 1500 capture the interdecadal temperature variability much better than does the full set of NWNA chronologies).

For the composite regions (HILAT and LOLAT), the difference

between the interannual and interdecadal correlations is very marked. This is because the common climate signal at these large spatial scales has relatively greater multidecadal power (i.e., a redder spectrum) than at the individual regional scale. On the basis of their correlation with modern temperatures, these results indicate that the MXD data set captures more than 60% of the decadal to multidecadal variability of the mean temperature of much of the Northern Hemisphere extra-tropical land masses, over the entire period from 1400 to present. Note that we have not considered the possible degradation of the climate signal due to the smaller number of tree cores comprising each chronology in the early part of the data set (it is not possible to estimate this effect by using a similar fixed-grid approach, since many of the individual tree cores do not span the correlation period of 1881–1960).

The reconstruction potential of the TRW data is at its maximum for the largest regional and near-hemispheric scales, but remains below that of the MXD data. The latter are used here, therefore, to reconstruct regional temperatures (although the additional skill that can be obtained from a combination of both variables will be considered elsewhere). The regional MXD time series, generated as described earlier, are calibrated against the regional April–September temperatures over the period 1881–1960, via a simple linear regression (Figure 11). The calibration parameters (Table 1) are used to estimate uncertainty ranges for each reconstruction. The uncertainty ranges are both time-dependent (due to the changing numbers of chronologies as demonstrated in Figure 10) and timescale-dependent (results in Figure 11 are at the decadal timescale), and they combine the uncertainty in the regression parameters with the strength of the residual temperature variability not captured during calibration. Full details are given in the Appendix.

The decadal variability is clearly well captured by the MXD data set, particularly for the NEUR, SEUR, NSIB, NWNA and ECCA regions (Figure 11, a, b, c, h and i). The poor correlation for the TIBP region results in the low variability of the reconstruction (Figure 11f), although this is a poorly sampled region in terms of chronologies and instrumental data. The lack of century-scale variability is clear during the calibration period of NWNA (Figure 11h). Some of the stronger decadal fluctuations show synchroneity across regions (e.g., the cool periods 1695–1700, 1810–20). Variability on a century timescale and longer will be partly suppressed by the standardization of the individual tree cores, as described in the earlier section on data, and is compared with an alternative processing approach by Briffa *et al.* (2001). A deviation between reconstructed and observed temperature during the most recent three or four decades is apparent in NEUR, NSIB, ESIB, CAS, NWNA and ECCA. This deviation was identified by Briffa *et al.* (1998b) and is discussed further in the next section.

For the ALL region, the annual and decadally smoothed reconstructions are both shown (Figure 12). The excellent correspondence between MXD and temperature at the interannual timescale is clear (Figure 12a), as is the increasing deviation between the two, particularly since about 1970 (although perhaps starting as early as 1935). The annual values (Figure 12b) are similar to the results of Briffa *et al.* (1998a), although they now benefit from an improved calibration procedure and an assessment of the uncertainty in the temperature reconstruction (which implies, for example, that, although the coolest summer was most likely to be 1601, the 1601 range of values does overlap with the ranges from other years). The widening of the uncertainty ranges in the earlier part of the reconstruction is more apparent for the decadally smoothed reconstruction (Figure 12c).

Recent declines in ring width and density

Briffa *et al.* (1998b) show that the decline in maximum latewood density that was evident over recent decades (Figures 11 and 12) is also apparent in the total ring-width data. For both MXD and TRW, the decline is strongest in the higher-latitude regions. Briffa *et al.* (1998b) discuss various causes for this decline in tree-growth parameters, and Vaganov *et al.* (1999) suggest a role for increasing winter snowfall. We have considered the latter mechanism in the earlier section on chronology climate signals, but it appears likely to be limited to a small part of northern Siberia. In the absence of a substantiated explanation for the decline, we make the assumption that it is likely to be a response to some kind of recent anthropogenic forcing. On the basis of this assumption, the pre-twentieth century part of the reconstructions can be considered to be free from similar events and thus accurately represent past temperature variability.

To avoid having to make the above assumption, an explanation for the decline is required. To search for an explanation is beyond the scope of this paper, but the earlier comparisons with monthly climate can be expanded to consider the possibility of a change in the seasonality of the tree response. Briffa *et al.* (1998b) demonstrate that the decline in MXD and TRW impacts most strongly upon the correlation between tree parameter and temperature at the regional spatial scale and the interdecadal temporal scale. For both MXD and TRW, the correlations between decadally smoothed regional time series and regional temperatures are computed for two overlapping periods: 1901–50 and 1935–84. These correlations show various changes between the periods, but are quite noisy and the significance of the differences is difficult to infer given the few degrees of freedom in the smoothed data. The changes become much clearer if the correlations are subsequently averaged across the five higher-latitude regions that exhibit the decline most strongly (because the standard error of the mean of five independent correlations is a factor $\sqrt{5}$ smaller than the standard error of the individual correlations). For MXD, the decadal high-latitude correlations show the dominance of the May to September temperatures (Figure 13a), and that the change in correlation from the early period to the later period is stronger in early summer (May to July) than in the late growing season (August and September). The results do not identify a new response season that becomes stronger in the later period, just that the existing response season weakens, particularly in the early to mid-season. For TRW (Figure 13b), the reduction in the decadal correlations is very strong for the growing-season mean temperatures. For the individual months, the results are a little more complex than for MXD, with a reduction in correlation for May, and July to September, but no change for June. The key result for TRW is that, again, there is no new response season emerging that could explain the decline in terms of a seasonality shift.

Despite the decline in tree-ring density, relative to the growing-season temperature, it is evident in Figure 12a that the interannual variations remain correlated for the 'ALL' region. This is investigated further by high-pass filtering (using a 10-year Gaussian-weighted filter) the regional MXD and temperature series, and then correlating them within a 20-year sliding window (Figure 14). As with all sample statistics, intrinsic variations are expected due to random sampling variations. A Monte Carlo approach is used, therefore, to identify those sliding correlations that deviate significantly from the mean correlation for each region. The shading in Figure 14 indicates the empirically identified ranges within which 90% of the correlations would be expected to fall (the ranges are skewed, being wider on the lower side compared to the higher side). For most regions, 90% of the correlations do indeed fall within the shading, indicating that the density-temperature relationship is maintained throughout. The 'ALL' region, for example, shows that the relationship is sustained even into the period of the recent decline in MXD. A notable exception to this is shown in the very low correlations prior to 1890 for the ECCA regional series, but these can be attributed to reduction in the coverage of Canadian temperature observations during this

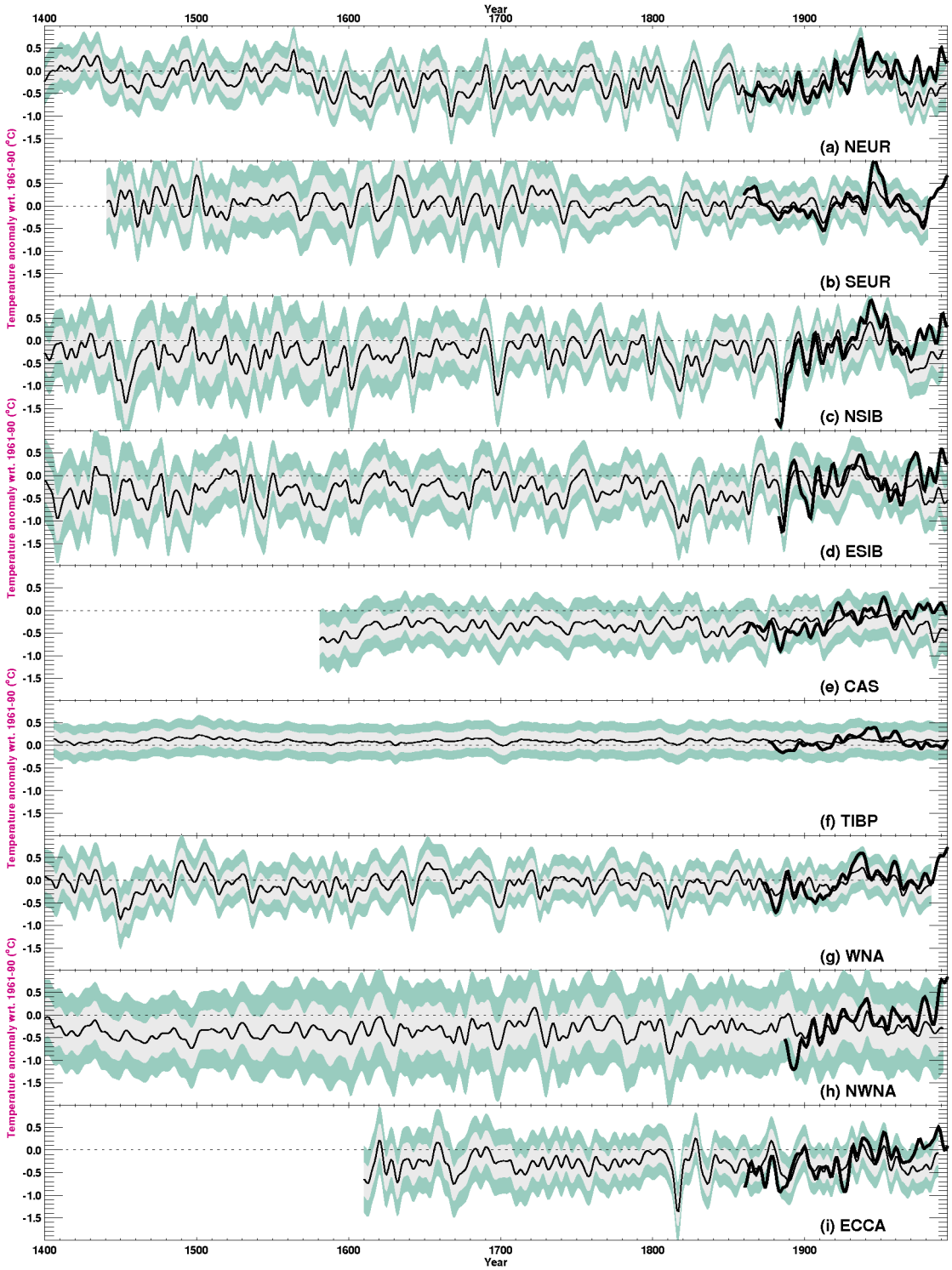

Figure 11 Reconstructions (thin lines, with shading to indicate ±1 and ±2 standard errors) and observations (thick lines) of regional-mean April to September temperatures (°C anomalies with respect to the 1961–90 mean) from 1400–1994 for nine regions. All values are decadally smoothed.

early period. For recent decades, NEUR and NWNA high-frequency correlations fall below the 5% threshold (and approach it for NSIB): these changes indicate the possibility that the high-frequency relationship with temperature is also being weakened, although it could simply be a result of the rapid decrease in the number of chronologies available near to the end of each regional record. Further sampling to update these records is required to investigate whether this is the case.

Summary and conclusion

The climate signal recorded in a network of 387 high-latitude or high-elevation tree-ring chronologies has been identified. The network comprises almost 10000 individual tree cores, and chronologies range in length from 85 to over 600 years. The chronologies of maximum latewood density show a strong and spatially coherent response to growing-season temperature, a sig-

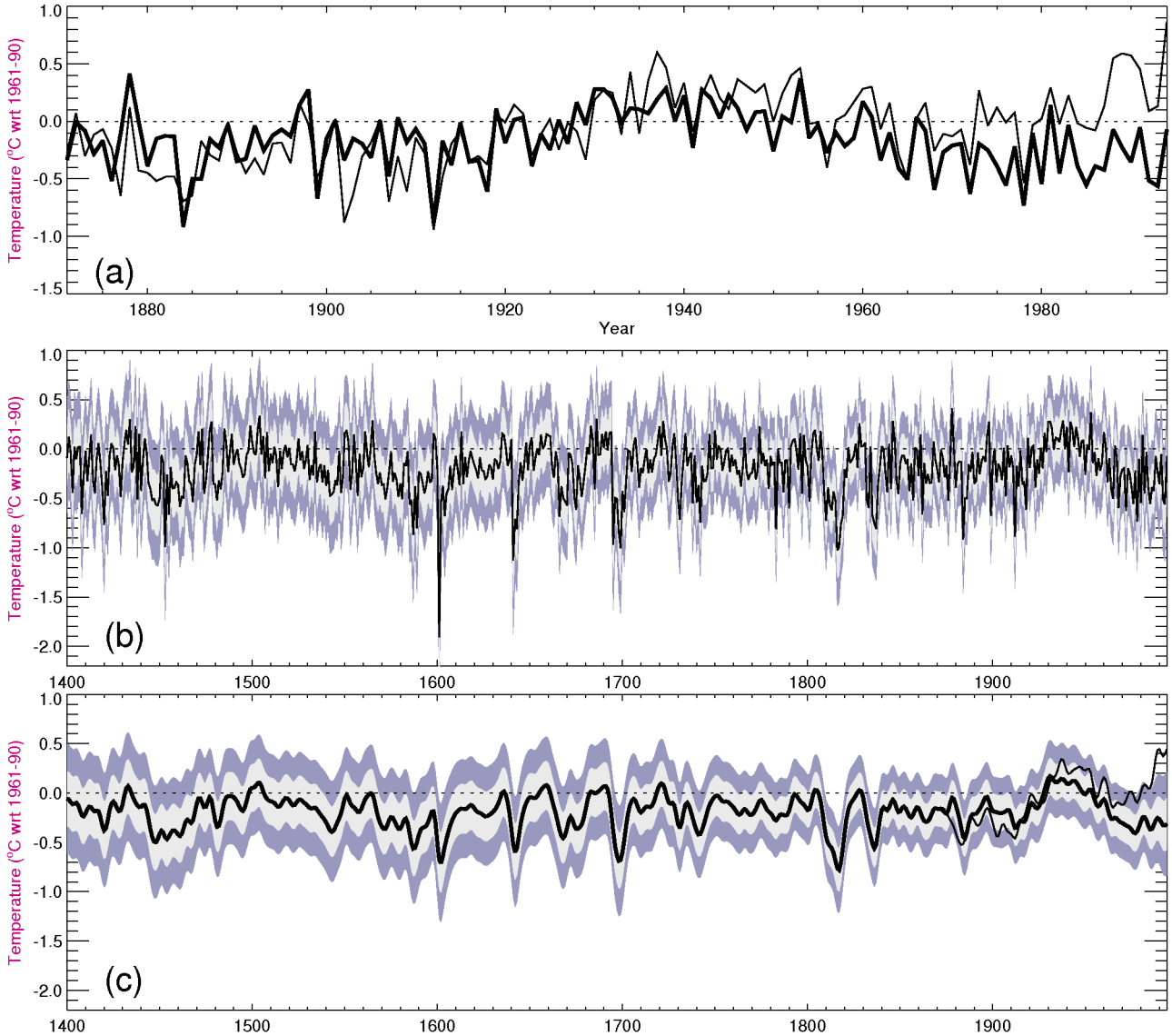

Figure 12 Observed (thin lines) and reconstructed (thick lines, with shading to indicate ±1 and ±2 standard errors) of the mean April to September temperature averaged over all grid boxes with chronologies in them. (a) Raw values from 1871–1994, with no error ranges shown; (b) raw values from 1400–1994 with no observed values; and (c) decadally smoothed values from 1400–1994.

Table 1 Calibration statistics for the regional April to September temperatures, reconstructed using regional MXD time series. Correlation (r), standard deviation of the residual temperatures (i.e., root mean squared error, rmse), and lag-1 autocorrelation of the residual temperatures (residual r_1)

Region	r	rmse (°C)	residual r_1
NEUR	0.84	0.37	0.11
SEUR	0.72	0.33	0.26
NSIB	0.76	0.59	0.06
ESIB	0.61	0.60	0.10
CAS	0.56	0.36	0.26
TIBP	0.36	0.21	0.41
WNA	0.74	0.34	0.23
NWNA	0.60	0.48	0.58
ECCA	0.75	0.45	0.15
ALL	0.76	0.22	0.31

nal that is further strengthened by forming regional averages (most correlations then exceed 0.7). The timing and length of the growing-season temperature to which the trees respond varies spatially, but an optimal common season is the mean for April to September. The total ring-width chronologies show, overall, a much weaker response to temperature forcing. The optimal temperature season is much shorter (June–August), although more than half of the chronologies do not show a significant correlation with the local grid-box June-to-August temperature. If the chronologies that do not appear to be temperature-sensitive are discarded, and the remainder formed into regional averages, then the total ring-width record provides a much improved representation of summer-temperature variations. Indeed, for the near-hemispheric scale, the total ring width has a correlation with June–August temperature ($r = 0.66$) that approaches the correlation between maximum latewood density and April–September temperature ($r = 0.76$).

The implication is that the weak temperature response of TRW can be partly explained as a weaker signal-to-noise ratio for TRW

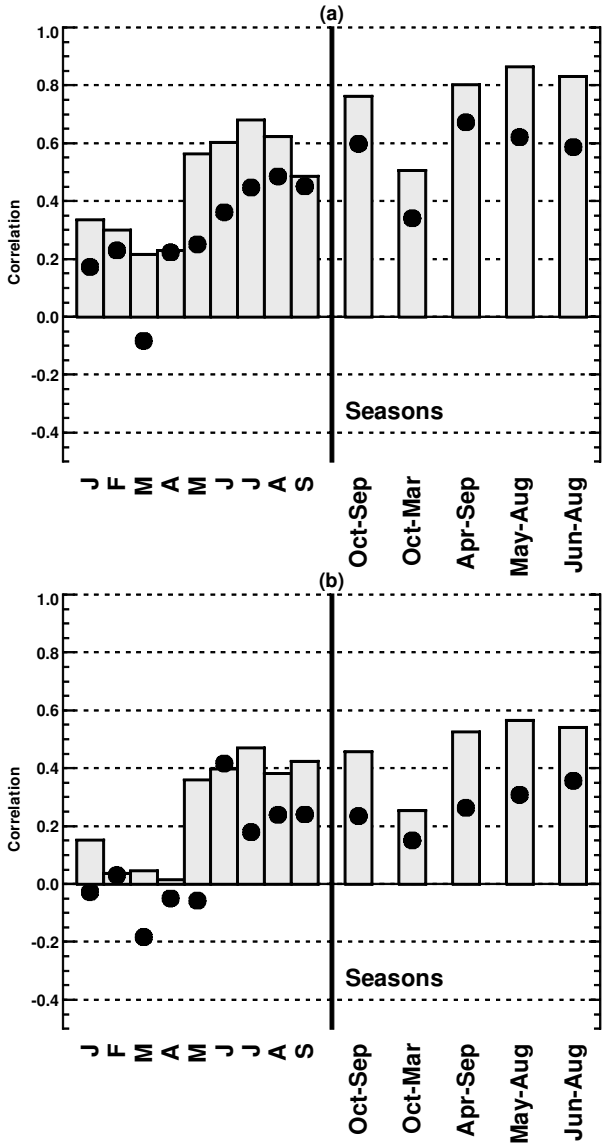

Figure 13 Correlations between regional-mean temperature and regional-mean (a) MXD and (b) TRW, computed for NWNA, ECCA, NEUR, NSIB and ESIB and then averaged to produce mean regional correlations for the high latitudes. All regional means were decadally smoothed prior to correlation. Correlations were computed separately for 1901–50 (bars) and 1935–84 (dots), against monthly and seasonal temperatures during the year of growth.

compared to that for MXD; the regional averaging strengthens the signal-to-noise ratio through the cancelling of uncorrelated noise. If sufficient material is available for sampling at each site, then additional ring-width measurements could be made (with less expense than density measurements) to improve the signal-to-noise ratio and hence the temperature signal.

For the present data set, however, the additional samples necessary to improve the quality of a reconstruction based on total ring width are not available, so only maximum latewood density is used to reconstruct temperature. Reconstructions of regional-mean temperatures have been developed here, including time- and time-scale-dependent assessments of their uncertainty. Comparison with observed temperatures demonstrates the veracity of the reconstructions for annual to multidecadal climate variations. It is not possible to verify the longer timescale variability in the reconstructions, but the standardization of the individual tree cores is likely to remove the century to multicentury timescale power. Briffa *et al.* (2001) present reconstructions based on an alternative technique for removing the bias due to changes in tree age, and compare them with those reported here.

The key result reported by Briffa *et al.* (1998b) is that there appears to be a non-temperature signal in the ring width and, particularly, in the ring density records that has strengthened over recent decades. This signal has a large impact on the correlation between the tree-ring variables and temperature *only* when considering regional averages or decadally smoothed variations. Here we show that the correlations are most affected during the first half of the growing season, providing support for some mechanism operating in the spring and early summer. The regional reconstructions are calibrated using pre-1960 instrumental observations because of this non-temperature signal in the maximum latewood density data.

Acknowledgements

This study was supported by the Commission of the European Communities (ADVANCE-10K, ENV4-CT95-0127) and the UK Natural Environment Research Council (GR3/12107). The early assembly of the tree-ring data set was supported by the Swiss National Science Foundation. We are grateful to Peter Bloomfield for discussions of reconstruction uncertainty and we thank Jonathan Palmer and Markus Lindholm for their comments on the manuscript.

Appendix: computing uncertainty ranges for reconstructions

The estimates of regional growing-season temperature constructed by simple linear regression (shown in Figures 11 and 12) include uncertainty ranges in terms of ± 1 and ± 2 standard errors about each estimated value. Each error range is based upon the uncertainty in the regression coefficients (the intercept, a, and the gradient, b) and the residual temperature variance (s^2) that is not captured by the regression-based reconstruction. The latter is typically the largest source of error in the reconstructions presented here, though the other terms can be non-negligible. The standard errors of the regression coefficients (SE_a and SE_b) are readily obtained (see, e.g., equations 1.4.5 and 1.4.2 of Draper and Smith, 1981). Given a time series of the predictor, $x(t)$, then the predicted temperature is simply

$$\hat{y}(t) = a + x(t)b \qquad \text{(A1)}$$

where the $\hat{}$ indicates that this is a prediction of the actual temperature, y. When the residuals from the regression are not autocorrelated, then the standard error of this prediction, SE_y, is given by:

$$[SE_y(t)]^2 = s^2 + SE_a^2 + [x(t) - \bar{x}]^2 SE_b^2 \qquad \text{(A2)}$$

where $\bar{x}$ is the mean of the predictors over the calibration period.

The uncertainty ranges are in fact timescale-dependent, and therefore need to be computed for each timescale at which the results are presented. Equation A2 is valid for the raw reconstruction, but in general a reconstruction might be presented after applying a smoothing function, replacing the value at time t by $\sum_i w_i \hat{y}(t-i)$, where the weights, w_i, sum to one. In Figures 11 and 12, we use a Gaussian-shaped smoothing operator. For the smoothed reconstruction, the standard error must be modified (Peter Bloomfield, personal communication) to give

$$[SE_y(t)]^2 = s^2 \sum_i w_i^2 + SE_a^2 + \left[\sum_i w_i [x(t-i) - \bar{x}] \right]^2 SE_b^2 \qquad \text{(A3)}$$

(comparing equations A2 and A3, note that the predictor anomaly is replaced by its smoothed value in the final term, but the more important change is that the first term is now scaled by the sum

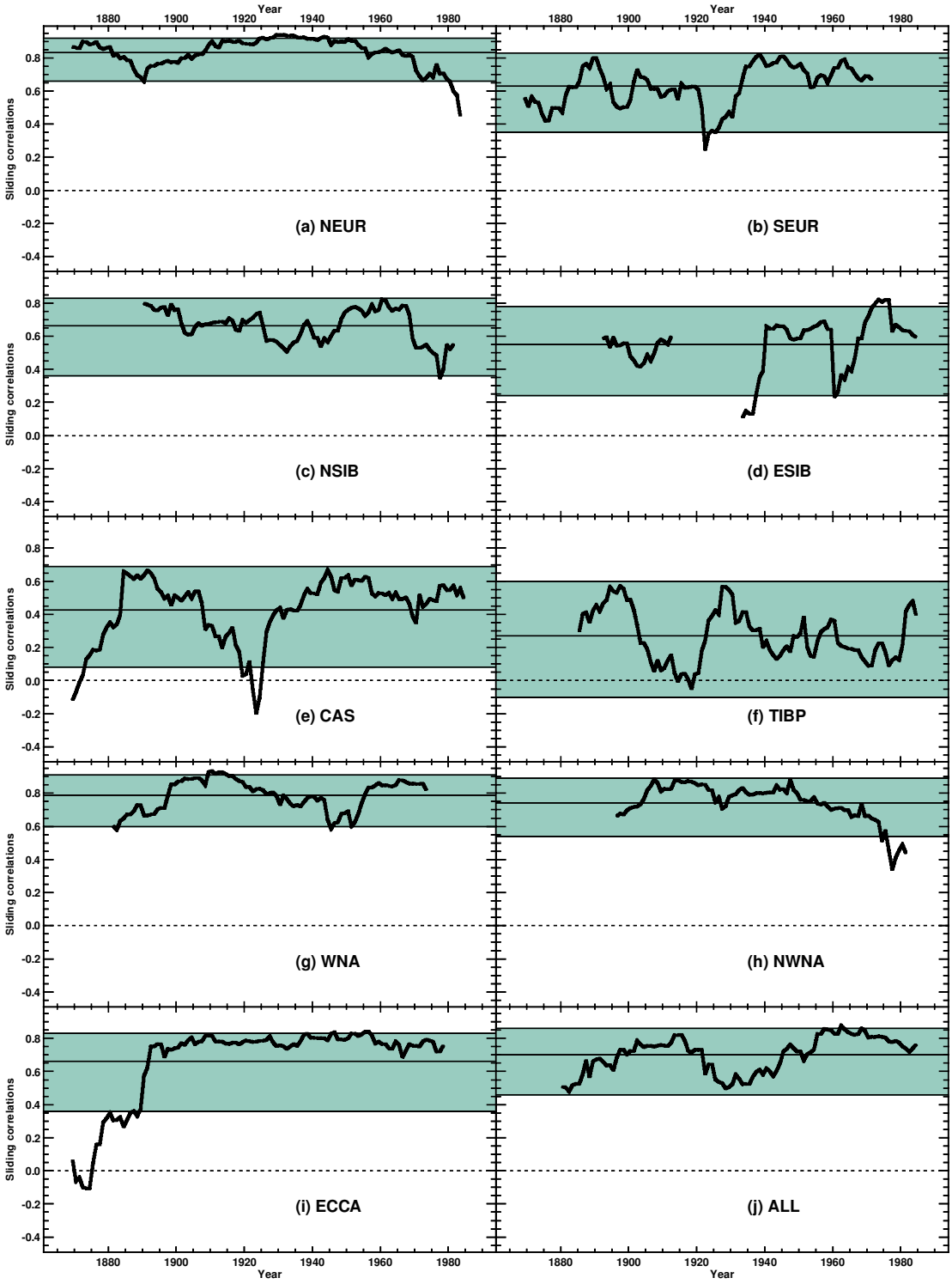

Figure 14 Correlations, in a sliding 20-year window, between regional-mean MXD and regional-mean April to September temperature, both high-pass filtered with a 10-year Gaussian-weighted filter, for the nine regions and for the composite 'ALL' region (based on all chronologies and all grid boxes with chronologies in them). The central horizontal lines indicate the mean of the correlations, with shading to show the 5 to 95 percentile range of sample correlations computed using a Monte Carlo model for a sample size of 20.

of squared weights, which is always < 1 and thus reduces the largest source of error).

An additional complication is that the residuals of the regression are generally autocorrelated. Significant autocorrelation increases the uncertainty surrounding the regression parameters. In addition, for the case where the standard error of a smoothed reconstruction (i.e., equation A3) is required, the reduction in the errors, as greater temporal smoothing is applied, is lessened as the autocorrelation increases. These effects are easily understood by considering reduced degrees of freedom and the averaging of correlated rather than uncorrelated values, but they are somewhat harder to quantify. A general solution of this problem would require information on the entire autocorrelation structure and the power spectrum of the residual series.

Conservative (i.e., upper-bound) results, however, can be estimated more simply (Peter Bloomfield, personal communication). A modification factor is defined as $\gamma = (1 + |\rho|)/(1 - |\rho|)$, where ρ is the lag-1 autocorrelation coefficient of the residual time-

series. [This factor is based on the ratio of the power spectrum at zero frequency (assuming a first-order autoregression model for the residuals) to s^2.] In the case of significant autocorrelation, SE_b^2 is replaced in A2 and A3 by the value $\gamma\ SE_b^2$. For $\rho \neq 0$, $\gamma > 1$ and the uncertainty range is increased. For the case of a smoothed reconstruction, the first term on the right-hand side of equation A3 is multiplied by the same factor.

References

Blasing, T.J., Solomon, A.M. and **Duvick, D.N.** 1984: Response function revisited. *Tree-Ring Bulletin* 44, 1–15.

Bräker, O. 1981: Der Alterstrend bei Jahrringdichten und Jahrringbreiten von Nadelhölzern und sein Ausgleich. *Mitt. forstl. Bundesvers Anst Wien* 142, 75–102.

Briffa, K.R. and **Cook, E.R.** 1990: Methods of response function analysis. In Cook, E.R. and Kairiukstis, L.A., editors, *Methods of dendrochronology: applications in the environmental sciences,* Dordrecht: IIASA/Kluwer, 240–47.

Briffa, K.R. and **Jones, P.D.** 1993: Global surface air temperature variations during the twentieth-century: Part 2, implications for large-scale high-frequency palaeoclimate studies. *The Holocene* 3, 77–88.

Briffa, K.R., Jones, P.D., Schweingruber, F.H., Karlén, W. and **Shiyatov, S.G.** 1996: Tree-ring variables as proxy-indicators: problems with low-frequency signals. In Jones, P.D., Bradley, R.S. and Jouzel, J., editors, *Climatic variations and forcing mechanisms of the last 2000 years*, NATO ASI Series 141, Berlin: Springer, 9–41.

Briffa, K.R., Jones, P.D., Schweingruber, F.H. and **Osborn, T.J.** 1998a: Influence of volcanic eruptions on Northern Hemisphere summer temperature over the past 600 years. *Nature* 393, 450–55.

Briffa, K.R., Osborn, T.J., Schweingruber, F.H., Harris, I.C., Jones, P.D., Shiyatov, S.G. and **Vaganov, E.A.** 2001: Low-frequency temperature variations from a northern tree-ring-density network. *Journal of Geophysical Research* 106, 2929–41.

Briffa, K.R., Schweingruber, F.H., Jones, P.D., Osborn, T.J., Shiyatov, S.G. and **Vaganov, E.A.** 1998b: Reduced sensitivity of recent tree-growth to temperature at high northern latitudes. *Nature* 391, 678–82.

Cook, E.R., Briffa, K.R., Meko, D.M., Graybill, D.S. and **Funkhouser, G.** 1995: The 'segment length curse' in long tree-ring chronology development for paleoclimatic studies. *The Holocene* 5, 229–37.

Cook, E.R., Briffa, K.R., Shiyatov, S.G. and Mazepa, V. 1990: Tree-ring standardization and growth-trend estimation. In Cook, E.R. and Kairiukstis, L.A., editors, *Methods of dendrochronology: applications in the Environmental Sciences*, Dordrecht: IIASA/Kluwer, 104–23.

Draper, N.R. and **Smith, H.** 1981: *Applied regression analysis.*, New York: John Wiley, 709 pp.

Fritts, H.C., Blasing, T.J., Hayden, B.P. and **Kutzbach, J.E.** 1971: Multivariate techniques for specifying tree-growth and climate relationships and for reconstructing anomalies in paleoclimate. *Journal of Applied Meteorology* 10, 845–64.

Hulme, M., Osborn, T.J. and **Johns, T.C.** 1998: Precipitation sensitivity to global warming: comparison of observations with HadCM2 simulations. *Geophysical Research Letters* 25, 3379–82.

Hughes, M.K., Vaganov, E.A., Shiyatov, S., Touchan, R. and **Funkhouser, G.** 1999: Twentieth-century summer warmth in a 600-year context. *The Holocene* 9, 629–34.

Jones, P.D. 1994: Hemispheric surface air temperature variations: a reanalysis and an update to 1993. *Journal of Climate* 7, 1794–802.

Jones, P.D. and **Briffa, K.R.** 1995: Growing season temperatures over the former Soviet Union. *International Journal of Climatology* 15, 943–59.

Jones, P.D., Briffa, K.R., Barnett, T.P. and **Tett, S.F.B.** 1998: High-resolution palaeoclimatic records for the last millennium: interpretation, integration and comparison with General Circulation Model control-run temperatures. *The Holocene* 8, 455–71.

Jones, P.D., New, M., Parker, D.E., Martin, S. and **Rigor, I.G.** 1999: Surface air temperature and its variations over the last 150 years. *Reviews of Geophysics* 37, 173–99.

Mazepa, V.S. 1999: Influence of precipitation on dynamics of annual radial increment in conifers of Eurasian subarctic regions. *Lesovedenie* 6, 14–21 (in Russian).

New, M., Hulme, M. and **Jones, P.D.** 2000: Representing twentieth-century space-time climate variability. Part II: development of 1901–1996 monthly grids of terrestrial surface climate. *Journal of Climate* 13, 2217–38.

Osborn, T.J., Briffa, K.R. and **Jones, P.D.** 1997: Adjusting variance for sample-size in tree-ring chronologies and other regional-mean timeseries. *Dendrochronologia* 15, 89–99.

Schweingruber, F.H. 1988: *Tree-Rings: Basics and Applications of Dendrochronology.* Dordrecht: Kluwer.

Schweingruber, F.H. and **Briffa, K.R.** 1996: Tree-ring density networks for climate reconstruction. In Jones, P.D., Bradley, R.S. and Jouzel, J., editors, *Climatic variations and forcing mechanisms of the last 2000 years*, NATO ASI Series 141, Berlin: Springer, 43-66.

Schweingruber, F.H., Briffa, K.R. and Jones, P.D. 1991: Yearly maps of summer temperatures in western Europe from AD 1750 to 1975 and western North America from 1600 to 1982: Results of a radiodensitometrical study on tree rings. *Vegetatio* 92, 5–71.

Vaganov, E.A. and **Shashkin, A.V.** 2000: *Tree-ring growth and structure in conifers.* Novosibirsk: Nauka, 238 pp.

Vaganov, E.A., Hughes, M.K., Kirdyanov, A.V., Schweingruber, F.H. and **Silkin, P.P.** 1999: Influence of snowfall and melt timing on tree growth in subarctic Eurasia. *Nature* 400, 149–51.